SAND98-2756J

EFFECTIVE USE OF MOLECULAR RECOGNITION IN GAS SENSING: RESULTS FROM ACOUSTIC WAVE AND *IN-SITU FTIR* MEASUREMENTS

Andreas Hierlemann[1*], Antonio J. Ricco[1*], Karl Bodenhöfer[2] and Wolfgang Göpel[2]

[1]Microsensor Research & Development Department, Sandia National Laboratories

Albuquerque, New Mexico 87185-1425, Phone: (505) 284 4248, Fax: (505) 844 1198,

e-mail: ahierle@somnet.sandia.gov

[2]Institut für Physikalische und Theoretische Chemie, Universität Tübingen,

Auf der Morgenstelle 8, 72076 Tübingen, Germany

KEYWORDS:

chemical sensor, molecular recognition, volatile organic compound (VOC), FTIR/SAW measurement, acoustic wave sensor, SAW sensor, TSMR sensor, polymer film, π stacking, metal coordination, cage compound.

* corresponding authors

DISCLAIMER

ABSTRACT

To probe directly the analyte/film interactions that characterize molecular recognition in gas sensors, we recorded changes to the *in-situ* surface vibrational spectra of specifically functionalized surface acoustic wave (SAW) devices concurrently with analyte exposure and SAW measurement of the extent of sorption. Fourier-transform infrared external-reflectance spectra (FTIR-ERS) were collected from operating 97-MHz SAW delay lines during exposure to a range of analytes as they interacted with thin-film coatings previously shown to be selective: cyclodextrins for chiral recognition, Ni-camphorates for Lewis bases such as pyridine and organophosphonates, and phthalocyanines for aromatic compounds. In most cases where specific chemical interactions—metal coordination, "cage" compound inclusion, or π stacking—were expected, analyte dosing caused distinctive changes in the IR spectra, together with anomalously large SAW sensor responses. In contrast, control experiments involving the physisorption of the same analytes by conventional organic polymers did not cause similar changes in the IR spectra, and the SAW responses were smaller. For a given conventional polymer, the partition coefficients (or SAW sensor signals) roughly followed the analyte fraction of saturation vapor pressure. These SAW/FTIR results support earlier conclusions derived from thickness-shear mode resonator data.

INTRODUCTION

High chemical selectivity and rapid reversibility can place contradictory constraints on the desired interactions between chemical sensor coating materials and analytes. Low-energy, perfectly reversible (physisorptive) interactions generally lack high selectivity, while chemisorptive processes, the strongest of which result in the formation of new chemical bonds, offer selectivity, but are inherently less reversible. One solution to this problem is to use arrays of sensing materials together with pattern recognition methods to obtain a pattern that provides selectivity from a set of individually nonselective materials [1-4]. Another solution is to discover or develop fully reversible "intermediate" interactions, lying at the weak end of chemisorption (< 120 kJ/mol), but exceeding simple

physisorption (0 – 30 kJ/mol). Systems that achieve this are often characterized by a spatially organized collection of physical interactions, i.e., the molecular shape and/or size specificity that results when a single host site interacts with a guest molecule through multiple van der Waals, metal-ligand, and/or hydrogen bonds, the cumulative energy of which falls in the desired 30 – 120 kJ/mol range. Sensor coating materials capable of such "molecular recognition" can play an important role in devising a selective and reversible system.

In the context of gas-phase chemical sensors, the meaning of molecular recognition, along with methods for its effective application, warrants discussion. Lehn *et al.* state that molecular recognition "implies a structurally well-defined pattern of intermolecular interactions" [5]: two species must complement one another in size, shape, and binding or functionality [6,7]. The maximum level of specificity, as realized in biological systems using lock-and-key interactions, is difficult to duplicate in gas/film interactions, where (1) the process of binding has a significant entropic component (largely independent of both coating and analyte), due to the change of the analyte's phase from gas to solution, and (2) the reversible changes in solvation that accompany, for example, the reorientation of a protein or the coordination of an ion, are particularly difficult to realize. Nonetheless, clever design of the overall sensing "scheme" can compensate for these handicaps.

Thus, we believe the pragmatic approach is to design a multisensor system that utilizes materials exhibiting enhanced sensitivity and selectivity for individual (or a single class of) target analytes due to specific or preferential intermolecular interactions. This approach is fully consistent with the definitions of molecular recognition in the previous paragraph [5-7], even though it often does not agree with the notion that molecular recognition implies selectivity ratios of 100 or more; the elegance of the multisensor approach is that "weak" or "moderate" molecular recognition, with selectivity ratios as low as two or even less, can be used effectively. In any case, molecular recognition can be proved using an independent means of characterizing the specific host/guest interactions; this is the motivation for the in-situ FTIR studies reported in this article. The utility of molecular recognition in such a case may be, in part, the ability to draw

directly upon well-understood chemical affinities to guide the selection of the coating materials comprising an array [3].

A very special case of molecular recognition is the detection of enantiomers, which is not possible using conventional, non-chiral polymers. For example, the two enantiomers of different analytes have been differentiated, and even quantified accurately in enantiomeric mixtures, by comparing the responses from a pair of coatings based on the complementary enantiomers of chiral amides [8]. This is not a precise embodiment of "perfect recognition using one coating for one analyte," because the sensor responses from the two enantiomeric coatings differ by as little as 10 – 30%, but the end result is highly effective enantiospecific recognition of a particular compound. Enantiospecific detection has also been established using supramolecular cages such as cyclodextrins [9].

In addition to direct evidence from spectroscopic measurements of specific interactions, the overall sorption characteristics of molecular recognition materials generally differ fundamentally from those of conventional polymers; this is illustrated by the thickness-shear mode resonator (TSMR) results reproduced in Figure 1 [9]. When the sorption isotherm is examined, molecular recognition results in pronounced nonlinearity—basically, Langmuirian behavior—in the low-concentration range where preferential sorption sites are being filled. This is displayed in Figure 1 for the concentration-dependent responses (isotherms) of a TSMR coated with a modified γ cyclodextrin supported in a matrix of poly(dimethylsiloxane) (labeled "50% w/w CD in SE 54"). The response to the R and S enantiomers of methyl lactate are shown by open and filled squares, respectively. Above the concentration (in Figure 1, about 750 μg/L, or $p/p_0 = 2\%$; p_0 is the saturation vapor pressure) where all the preferential sites are occupied, the behavior of a molecular recognition coating resembles that of a conventional polymer: the sorption isotherm is linear until a high enough concentration is reached that Henry's law is no longer valid [8]. This can occur for fractional saturation (p/p_0) values as low as 5% or as high as 15%, at which point non-unity activity coefficients must be accounted for; at the upper limit of concentration in Figure 1 (corresponding to $p/p_0 = 7\%$), this limit has not yet been reached. If Henry's Law continues to apply at high concentrations, it will ultimately fail when multilayer

condensation on the outer surface contributes significantly to the response (most apparent for very thin films). In addition, there is an inevitable additive contribution from nonspecific sorption in the coating layer, even at low concentrations, because it is generally impossible to design a film that has only specific sorption sites. The equilibrium coefficients for partitioning into the molecular recognition film for the specifically detected target analytes at low concentrations (usually below 1 - 2% of p_0) are typically 5 – 100 times larger than those of nonspecifically recognized analytes (at equivalent p/p_0), or those of the specifically detected analytes sorbed by conventional organic polymers. We note, however, that the presence of a shape-, size-, or functionality-specific interaction does not automatically imply a far stronger interaction than "simple" physisorption. In most cases, inclusion into cage compounds, for example, is a consequence of the "normal" spectrum of physical and very weak chemical interactions: Van der Waals, hydrogen bonding, and weak electrostatic or coordination bonds. It is the geometrical arrangement of several to many such interactions in a single host that provides a significantly stronger interaction for certain orientations, shapes, and/or sizes of analyte molecules.

In contrast to the chemically and chirally specific interactions suggested by the CD isotherms, Figure 1 also shows the isotherms for the two methyl lactate enantiomers sorbed by the chemically nonspecific conventional polymer polyetherurethane (PEUT; indicated by "–" and "x" for the R and S enantiomers). The responses are very linear all the way up to 2500 µg/L (p/p_0 = 7%), with a zero intercept, consistent with Henry's Law: simple physisorptive behavior.

There are a number of reports in the literature of shape or class selectivities attributed to sorption of analytes by cage compounds [10-13]. Some of these, however, show "selectivities" correlated more strongly with key thermodynamic properties of the investigated analytes (saturation vapor pressure, for example), than with the presence of a demonstrated specific interaction or recognition process. Consequently, the general idea of molecular recognition in gas sensors was questioned recently by Grate *et al.* [14]. Nonetheless, we recently presented convincing evidence for specific recognition of particular target analytes, including the discrimination of enantiomers using

supramolecular cages [9] and the detection of Lewis-basic, nitrogen-containing volatile organic compounds (VOCs) using metal coordination [15]; ongoing investigations of phthalocyanines provide further evidence for effects of specific recognition [16]. In this paper, we present detailed molecular spectroscopic evidence to support our claims of specific interactions for several coating materials and analytes.

We systematically investigated three coating materials, depicted in Figure 2, previously shown to be selective for gas sensors [9,15,16], and offering three different types of reversible interactions stronger than simple physisorption:

- bucket-like supramolecular compounds, in this case the cyclodextrins (CDs). Here, oriented adsorption of the analyte molecules within the CD torus (inclusion of the analyte molecule in the supramolecular cage) appears to control the recognition process. Since the γ-cyclodextrin derivative used here has a large cavity, and the torus is not rigid, the determining factor is not simple shape or size selectivity. These cage compounds were used earlier as coatings on TSMRs to demonstrate chiral recognition with gas sensors [9].
- soluble phthalocyanines (films are composed of the pure polycrystalline material). The specific interaction is most likely "π stacking", an intense interaction between the large, delocalized π-electron systems of the phthalocyanines and those of volatile aromatic analytes such as benzene, toluene, and xylene (BTX) [16].
- metal coordination compounds, represented here by Ni camphorates (films are composed of the pure polycrystalline material). In the case of Ni camphorate, the specific interaction is probably a coordinative ligand-metal donor bonding of oxygen- or nitrogen-containing analytes to the Ni atom of the chelate complex. Note that the two water molecules shown in Figure 2 are highly labile; previous studies with coordinatively unsaturated Cu^{2+} shows that such ligands can readily be displaced by analytes [17]. Such coordination compounds can be used, for example, for the specific detection of the bases DMMP (dimethylmethylphosphonate) or pyridine under conditions of somewhat slow (minutes) but complete reversibility [15].

To understand these specific interactions in more detail, we performed combined SAW/*in-situ* FTIR-ERS measurements, using the experimental setup shown in Figure 3. During each experiment, the film-coated SAW device, the inter-transducer region of which additionally acts as a reflector for the IR beam at grazing incidence, is exposed to various VOCs. From simultaneously recorded changes in the device frequency (principally due to mass changes) and changes in the IR spectrum of the VOC, we were able to draw some fundamental conclusions about the coating/analyte interaction processes. Appropriate control experiments, using conventional organic polymers expected to show only simple physisorption interactions with the analytes, were conducted for comparison and validation of the results.

The fundamentals of FTIR-ERS of organic thin films are described elsewhere [18-22]. Generally, FTIR-ERS on Au substrates is sensitive to both the polarization state and angle of incidence of the infrared radiation [18-20, 23]. The reflectivity of the applied gold layer at different incident angles of the IR beam is detailed elsewhere [24]. The sum of the incident and image (in the surface of the metal) electric vectors for *s*-polarized infrared radiation produces essentially no electric field at the film/Au interface at all angles of incidence, which prevents IR absorption by any near-surface dipole. In contrast, the vectors of the incident and image electric vectors for *p*-polarized IR radiation are additive, resulting in an electric field with a nonzero component perpendicular to the surface, with a maximum amplitude measured at near-grazing (for gold, >89.5° from normal) incidence [18-20, 23]; for practical reasons, experimental measurements are made at ~ 80 – 85° from normal. Thus, surface-confined or near-surface molecules having a dipole component oriented perpendicular to the surface absorb only *p*-polarized IR radiation (the so-called "surface selection rule"). To enhance the magnitude of the signal, particularly for anticipated subtle spectral changes, however, we applied relatively thick layers of the sensitive coating materials (0.5 – 1 μm; the surface selection rule applies within approximately one-quarter wavelength of the surface, or 2.5 – 0.7 μm for the 1000 – 3500 cm^{-1} range [25]). In addition, the films were deposited using spray coating, which results in grainy or pebbly films with high surface area (speeding absorption), randomly oriented surface features (eventually causing multiple reflection or

scattering), and no overall molecular order within the film. Hence, *s*-polarized IR radiation was absorbed by all the coating materials as well, but with markedly lower absorbance than for the *p* wave. For both polarizations, the analyte molecules in the gas phase also absorb IR radiation, contributing to the total signal. Therefore, appropriate background spectra using both polarization states for each coating material and for each gas-phase analyte (at multiple concentrations) were first acquired for reference purposes. We then compared separately the *p*- and *s*-polarized reference spectra of the gaseous analytes over a bare gold reflecting surface to the correspondingly polarized spectra of the analytes sorbed by the selective-film-coated Au surface, after first subtracting the spectra of the selective coatings under a nitrogen purge as background.

The SAW devices consist of five parallel sets of input and output interdigital transducers formed on an extra large piezoelectric quartz substrate (Figure 3) [26] to accommodate the gold reflection layer. An alternating voltage applied to each input transducer launches a Raleigh wave that traverses the crystal surface. The output transducer converts the wave back into an electrical signal. Any change in a physical property of the SAW device or a film overlay on the surface that affects either (or both) of the wave propagation parameters, velocity and attenuation, can be exploited to construct a sensor [27]. If the SAW velocity is perturbed only by mass loading variations; the change in frequency, Δf, is related to the change in sorbed mass per area, $\Delta(m/A)$, by

$$\frac{\Delta f}{f_0} = -\kappa c_m f_0 \cdot \Delta(m/A), \qquad (1)$$

where c_m is the mass sensitivity coefficient (1.33 cm^2/g-MHz for ST-quartz [28]), f_o is the unperturbed oscillator frequency (97 MHz), and κ is the fraction of the center-to-center distance between the transducers covered by the chemically sensitive film [27]. In addition to mass-loading effects, changes in the velocity and attenuation of the surface acoustic wave can result from changes in the viscoelastic properties of surface-confined layers [27,28].

In addition to the SAW/FTIR devices, we used TSMRs to precisely assess the partition coefficients of the various VOCs. The setup consisted of discrete thickness-shear mode resonators operating at a fundamental frequency of 30 MHz. As shown by Sauerbrey [29], the vibrating frequency of a quartz crystal changes, to a first approximation, in proportion to the mass deposited onto or removed from the surface (the form of the Sauerbrey equation is identical to Eq. 1, with the constraint that 100% of the active surface be uniformly affected by the change in mass and $\kappa = 1$ [27]). Because both the analyte concentrations and the TSMR fundamental frequency are rather low (30 MHz), and the acoustic wavelength is fairly long (110 μm) compared to the coating thicknesses, viscoelastic effects are assumed to contribute only to a small extent to the frequency change due to gas sorption [30]. Any changes in the conductivity of the sensing material would affect neither the SAW nor TSM device response, because in both cases the thin film is on top of a uniform gold film that shorts out the electric field associated with the acoustic wave [27]. Further details of acoustic wave-based mass-sensitive devices can be found in the literature [27,30-32].

EXPERIMENTAL DETAILS

Coating materials

The coating materials chosen for this study (Figure 2) were: a modified γ-cyclodextrin (3-*O*-butanoyl-2,6-di-*O*-*n*-pentyl-γ-cyclodextrin, CD) [33] as a cage compound, a nickel camphorate (Ni(II)-bis[(1R)-(+)-3-heptafluorobutanoyl-8-methylidencamphorate, Ni-Cam) [8] as a coordinatively unsaturated metal center, and a soluble nickel phthalocyanine (Ni-2,3,9,10,16,17,23,24-octakis(pentoxy)phthalocyanine, NiPC) [34] as a material with a large, delocalized π-electron system. CD and Ni-Cam were synthesized by the group of Prof. Schurig and NiPC was synthesized by the group of Prof. Hanack, both at the Institute of Organic Chemistry of the University of Tübingen. In addition, we used the polar polymer poly(etherurethane) (PEUT; Thermedics, Woburn, MA) [9] and the nonpolar polyisobutylene (PIB, MW ≈ 380,000; Aldrich, Milwaukee, WI) as conventional polymer coatings, nominally free of any molecular recognition moieties, for

comparison. The coatings on the SAW/FTIR-devices were prepared by spin casting from trichloromethane (chloroform) solutions or spray coating from dichloromethane solutions; layer thicknesses ranged from 500 nm to 1 μm.

To coat the TSMRs, the coating materials were dissolved in dichloromethane (concentrations ~1 mg/mL) and the solutions sprayed onto the cleaned devices with an airbrush using pure nitrogen as carrier gas. On-line monitoring of the frequency decrease allowed determination of the frequency shifts due to coating and calculation of the layer thickness, assuming a uniform and homogenous distribution of the polymer over the device surface. The measured frequency shifts due to the coatings were approximately 50 kHz (thickness ~ 250 nm).

Gas mixing

For TSMR testing, vapors were generated from specially developed temperature-controlled (T = 283-298 K) vaporizers using synthetic air as carrier gas and then diluted to known concentrations by computer-driven mass-flow controllers. The internal volume of these vaporizers was dramatically smaller than typical gas-washing bottles ("bubblers"), hence very small quantities of expensive chiral analytes could be released at constant concentration [35]. The absolute vapor-phase concentrations at the respective temperatures were calculated following the Antoine equation [36]. All vapors were mixed and temperature stabilized before entering the thermoregulated chamber. The measurements were performed at a constant temperature of 303 K. The thermostat used was a microprocessor-controlled Julabo FP 30 MH (Julabo, Seelbach, Germany). The gas flow-rate was 200 mL/min at a total pressure of 10^5 Pa. The response time of the sensors is typically < 1 s. However, the time necessary to reach an equilibrium state in this setup is about 3 minutes, the time required to change completely the gas concentration in the chamber (volume 20 mL) at the chosen flow rate. Typical experiments consisted of alternating exposures to air and vapor. Exposure times of 10 minutes were followed by 10 minutes purging the chamber with synthetic air.

For coated SAW/FTIR device testing, mass-flow controllers and solenoid valves, under computer control, supplied three gas streams: a pure N_2 carrier, which was

saturated with the analyte vapor using a gas-washing bottle with large-area frit, a mix-down stream, used to adjust analyte concentration from 0.05 – 99% of the analyte's saturation vapor pressure (p_0), and a dry N_2 purge stream. The analytes were vaporized at 293 K, whereas the measurement chamber and the sensors were maintained at 303 K. A p/p_0 value of 5% of, e.g., *n*-octane at 293 K hence corresponds to a p/p_0 value of 3% at 303 K (the proportionality factor depends on the nature of the analyte). Unless otherwise noted, in the following we report the p/p_0 values corrected to the measurement temperature of 303 K, at which the device and sensing film were maintained. The total flow rate through the custom-designed SAW/FTIR test fixture (described below) was 500mL/min. The temperature of the fixture and gas stream were maintained at 303 K.

Analytes

Most of the analytes were standard organic solvents and used as purchased from Sigma-Aldrich, Milwaukee, WI, without further purification. In addition, we used both enantiomers of methyl lactate (methyl 2-hydroxypropionate, purity > 98%, Aldrich) and both enantiomers of methyl 2-chloropropionate (Fluka Chemie AG, Buchs, Switzerland).

Thickness-shear mode resonators

The TSMR array consisted of discrete piezoelectric quartz crystals (AT-cut) with gold electrodes, operating at a fundamental frequency of 30 MHz (plate thickness: 55.6 μm), purchased from Kristallverarbeitung, Neckarbischofsheim, Germany [30]. Each crystal was powered by an oscillator circuit (bipolar, parallel resonance) constructed at the University of Tübingen; a single coaxial cable provides the supply voltage and transmits the frequency signal. A custom-developed scanner, compatible with signal frequencies between 100 kHz and 100 MHz, was controlled by a PCL 726 interface card (Labtech, Wilmington, MA) in an IBM-compatible PC-AT. This allowed for the sequential monitoring of each TSMR output by the computer using a Hewlett-Packard 5334B frequency counter interfaced via an IEEE-488 interface bus. Frequency differences, recorded every 30 s at 0.1 Hz resolution and using a 1 s gate time, are reported relative to

the initial, unperturbed value for each device. Sensor responses were taken as the frequency difference between analyte exposure and pure purge gas.

Surface acoustic wave devices

SAW delay-line devices were custom designed at Sandia National Laboratories to provide a large gold reflection area for the FTIR measurements in the center of the interaction region of the SAW delay lines (Figure 3). Five independent sets of input and output interdigital transducers (IDTs; 200 nm-thick Au on a 15 nm-thick Cr or Ti adhesion layer) were defined on a 41 x 15.5 mm ST-quartz substrate. The IDT periodicity (acoustic wavelength) of 32 μm yields a center frequency of 97 MHz; each IDT is comprised of 50 finger pairs; the acoustic aperture of each device is 50 wavelengths; the center-to-center IDT spacing is 312 wavelengths. Compared to the SAW delay lines used in the past in our laboratory [37], it was necessary to increase the center-to-center IDT spacing, in addition to using the large substrate that accommodates 5 identical delay lines, to provide a sufficiently large selective-film-coated Au reflection surface (8.5 x 40 mm in area, 200 nm of Au upon 15 nm of Ti or Cr) for the FTIR-ERS measurements. Only the three center delay lines were used for SAW measurements. Adjacent (parallel) SAW delay lines are separated by 6.5 mm (200 wavelengths), and a detailed frequency analysis of the operating characteristics of these devices revealed negligible cross-talk between adjacent delay lines. The response of the three independent SAW devices, therefore, could be measured simultaneously to provide redundant measurements during each analyte exposure. SAW measurements were performed according to previously described procedures [17,37,38]. The SAW/FTIR devices were mounted in a custom gas-flow test cell (Figure 3), which was attached to a gas manifold.

SAW/FTIR-ERS measurements

The combined SAW and FTIR-ERS measurements were performed using a custom-designed gas-flow test cell, shown in Figure 3 [26], that fits onto a "seagull" reflectance accessory that directs the incident and reflected beams from and to a commercial FTIR spectrometer (as described below). The flow cell consists of two stainless-steel body

components. The cover section has six SMB connectors allowing three independent SAW measurements, four O-ring-sealed window ports for 45°- and 80°-off-normal surface IR absorbance measurements, and two gas-flow ports. IR-transparent KBr windows were used for the studies discussed in this report. Spring-loaded "pogo" pins located at the bottom of this component are used to make low-resistance contacts with the Au bonding pads of the SAW devices. The base section contains a recessed region to accurately locate the SAW/FTIR-ERS device. It also has two liquid-flow ports, which are used to maintain the cell at a constant temperature during the combined measurements (303 K).

The FTIR-ERS measurements were performed using a Nicolet Magna-IR 750 spectrometer, including a KBr beamsplitter and a liquid N_2-cooled $Hg_xCd_{(1-x)}Te$ (MCT) detector. Spectra were obtained using a Harrick Scientific (Ossining, NY) Seagull reflection accessory, which may be configured for surface reflection experiments involving incident angles spanning the 5° to 87° range without the need for optical realignment. The optical design results in no polarization dependence on the angle of incident radiation. For the present study, all spectra were acquired using infrared radiation incident on the substrate at 80° from the surface normal. The orientation of the infrared radiation (e.g., *s*- or *p*-polarized) was controlled by rotating a wire-grid polarizer, placed in the incident beam, ±90°. The following parameters were used to acquire the spectra: spectral range, 500 - 4000 cm^{-1}; aperture, 35; mirror velocity, 0.9494 m/s; resolution, 1 cm^{-1}; boxcar apodization; number of scans, 100; collection time 160 sec. The interferograms were saved for each spectrum to allow reprocessing of the spectra if desired.

FTIR-ERS data were acquired for each of the three molecular recognition materials and two conventional polymers described above, in the presence of each one of a number of analytes, with thin films of each material coated over the Au reflecting pad (Figure 3) in the center of the FTIR-ERS/SAW device. The following protocol was used: (1) the test-cell containing the coated device was purged with N_2, (2) a *s*-polarized reference spectrum (*s*-background) was acquired, (3) the polarizer was rotated +90°, (4) a *p*-polarized reference spectrum (*p*-background) was acquired, (5) the SAW/FTIR-ERS

device was exposed to a target analyte, (6) a *p*-polarized sample spectrum was obtained in the presence of the gas-phase analyte (by subtracting the *p*-background), (7) the polarizer was rotated -90°, (8) an *s*-polarized sample spectrum was obtained (by subtracting the *s*-background). The *s*- and *p*-background-subtracted sample spectra were then compared to the gas-phase spectrum of the respective analyte, which had been previously obtained using an Au-coated FTIR/SAW device with no chemically sensitive layer. Additional spectra were acquired by repeating Steps 1 through 9 for at least 3 different concentrations of each analyte; concentrations were selected to achieve a reasonable IR signal intensity at the lowest possible gas-phase concentration which, practically, meant that the absolute vapor-phase concentrations were adjusted between 3000 and 5000 ppm (by volume) for all the solvents, regardless of the saturation vapor pressure, providing a roughly comparable IR absorbance from each gaseous analyte. The fraction of saturation vapor pressure (p/p_0) values at the vaporization temperature of 293 K hence ranged from 1% for trichloromethane to about 20% for tetrachloroethene, but all analyte concentrations were less than 10% of p_0 at the measurement temperature of 303 K.

For each coating material, two independent SAW/FTIR devices were prepared. After completing the set of measurements on one of the devices, a random sampling of analytes and concentrations was examined on the second device to confirm consistency of results.

RESULTS AND DISCUSSION

TSMR sorption isotherms: thermodynamic evidence for molecular specificity

Thermodynamic evidence for specific recognition mechanisms was obtained by recording TSMR responses over a wide concentration range. In some instances, the TSMR offers the advantage of more readily measuring "true" thermodynamic properties for the sorption of analytes by a thin film than some other types of acoustic wave device, e.g. the SAW. "Thermodynamic responses"—those directly proportional to the number of molecules in the film with a solely mass-dependent constant of proportionality—are generally obtained from acoustic wave devices supporting sorptive films that are

acoustically thin [28]. This is typically an easier criterion to meet for the TSMR than, e.g., the SAW, because (a) the wavelength is much longer for the TSMR, so a film can be thicker before it approaches a significant fraction of one acoustic wavelength, and (b) the film is less deformed by the largely in-plane motion of the TSMR device surface, in contrast to the elliptically polarized motion of the surface of the SAW device [28].

Figure 1 shows the response of several coated TSMRs upon exposure to methyl lactate over a wide concentration range. The reference sensor, coated with a nonspecifically interacting polymer (PEUT) exhibits linear concentration dependence with a zero intercept. Such linear sorption isotherms (Henry-type) are typical for physisorption processes [39]. The partition coefficient in this case is a temperature-dependent constant.

The sensor coated with 50% (w/w) CD (dissolved in a polysiloxane polymer matrix; for details see [9]) shows a fundamentally different response. The sorption isotherms for both enantiomers deviate significantly from linearity, the partition coefficients decreasing with increasing concentration. This isotherm shape indicates specific, preferential analyte/matrix interactions characterized by Langmuir-like saturation of binding sites at low concentrations, whereas at high concentrations the curves are nearly linear and the slopes are characteristic of physisorption. This behavior continues until Henry's Law fails and thermodynamic activity coefficients must be introduced due to nonlinearities in the sorption behavior. Hence, a typical sensor response isotherm for preferential sorption includes two main regions: Langmuir-type behavior dominating in the low concentration range, gradually giving way to linear Henry-type physisorption at moderate concentrations. Details of the modeling of such superimposed sorption isotherms and extraction of the respective thermodynamic parameters are discussed at length in [9].

The preferential sorption mechanism represented by the responses in Figure 1 is the occupation of the CD supramolecular cages by the analyte molecules. Similar nonlinear sorption behavior at low analyte concentrations occurs for each of the "molecular recognition" coatings reported on below. The coating materials and the corresponding "specifically detectable molecules" for which we have characterized the sorption process include: CD with methyl 2-chloropropionate; Ni-camphorate with

pyridine [15] and DMMP; and NiPC with aromatic compounds such as benzene, toluene, and xylene [16]. Similar results have been reported by other authors, e.g., for paracyclophanes [40]. We emphasize that, in the present context, the term molecular recognition does not imply any particular minimum value of the partition coefficient, nor even a minimum discrimination ratio relative to nonspecifically detected species. Rather, it implies a chemically specific coating/analyte interaction that is manifested in the sort of dual-mode sorption isotherm described above. Further, as we describe in detail in the following sections, such recognition can be spectroscopically detectable when the specific interactions involve moieties with sufficiently intense vibrational bands in a convenient spectral region. In the next sections, we discuss in detail the simultaneously recorded SAW and FTIR-ERS data and the independently determined TSMR partition coefficients for each of the three different types of molecular recognition coating.

Protocol for combined SAW/FTIR-ERS measurements

For each of the molecular recognition coating materials, several analytes expected to display specific chemical interactions with the coating materials were studied, and their vibrational spectroscopic and acoustic wave sensor responses were compared to those for a number of nonspecifically sorbed analytes. For analytes of both categories, interactions with the "ordinary" organic polymers polyisobutylene and polyetherurethane were also examined as controls. The following protocol was followed to obtain the results; additional details may be found in the Experimental Details section.

First, the gas-phase spectra (under separate *p* and *s* polarization) were recorded at two different concentrations, using a bare gold reflecting surface in the SAW/FTIR-ERS test cell (Figure 3). The reflection spectra of the bare gold surface under a nitrogen purge were subtracted as background. These gas-phase analyte spectra, which display essentially no difference between *p* and *s* polarizations, served as references when looking for spectral changes due to specific analyte/coating interactions.

The *p* and *s* spectra of all the sensor coating materials were also recorded (under a nitrogen purge), subtracting the background reflection spectrum from a bare gold device in each case. As expected, the intensities of the bands associated with the films were

much more intense for *p*-polarized spectra than for *s*, a consequence of the surface-selection rule (see the Introduction for explanation). These coating spectra served as a second reference to determine whether any of the observed spectral changes upon analyte sorption were associated with the coating materials.

Next, *s* and *p* spectra were recorded for each analyte sorbed by each of two "nonspecific" reference polymers, PIB (nonpolar) and PEUT (polar). The spectra of the analyte-free polymer-coated devices under a nitrogen purge were subtracted out as background, eliminating all bands associated with the analyte-free polymer coating materials. The resultant gas-phase analyte spectra were invariably identical to those recorded for a bare gold reflecting surface. This demonstrates the absence of any spectroscopically detectable specific interactions affecting either the analyte's or the reference polymer's vibrational structure. Thus, in the figures described below, the spectra labeled PIB and PEUT are in every case identical to the gas-phase spectra of the respective analyte.

Finally, spectra were acquired for all of the analytes sorbed by each of the molecular recognition coatings. The spectroscopic changes were essentially the same for both polarizations of the incident IR radiation, but much more intense in the *p* spectra than in the *s* spectra (the surface selection rule). Therefore, only the *p* –spectra are displayed in most cases. The changes in the IR signatures will be discussed in detail below. Generally, major changes in the spectra are not expected, since all the specific interactions are completely reversible simply by removal of the analyte from the ambient phase (accomplished by purging with pure N_2). The interactions are cumulative physical and/or weakly chemical in nature; no chemical reactions occur, no severe distortions of the molecules, nor any strong, irreversible interactions occur. Nonetheless, the minor spectroscopic changes we present below are clear and unambiguous evidence of chemically specific interactions between coating material and analyte.

Cage compound: modified γ-cyclodextrin (CD)

Both enantiomers of methyl lactate and of methyl 2-chloropropionate were examined due to the expectation of specific (chiral) interactions with the CD; these were

complemented by several reference analytes, expected not to interact specifically, but representing several chemical functionalities: *n*-octane, toluene, trichloromethane, tetrachloroethene, and propan-1-ol. In brief, chiral selectivity for R-methyl lactate over the S enantiomer was indicated by both the IR spectral changes and acoustic wave device results, and likewise for the related compound methyl 2-chloropropionate (though in this case the S enantiomer was preferred over the R); the conventional organic polymers displayed no chiral preference. The spectra of every analyte examined was the same when sorbed in PIB or PEUT as for the free analyte in the gas phase. The "reference analytes" listed above showed no changes in the IR spectrum, consistent with a general lack of selectivity displayed by the acoustic wave device results.

FTIR-ERS results. Figure 4 shows the relevant portions of the IR spectra of methyl lactate (i.e., methyl 2-hydroxypropionate) recorded simultaneously with the SAW response. From bottom to top, the absorbance spectra displayed are those of methyl lactate sorbed by PIB and PEUT ($p/p_0 = 2.7\%$; spectra are identical for R and S enantiomers), S-methyl lactate sorbed by CD ($p/p_0 = 2.7\%$), and R-methyl lactate sorbed by CD ($p/p_0 = 2.7\%$ and 5.4%). These spectra represent the raw data and have not been processed in any way.

The PIB and PEUT spectra in Figure 4 are identical to the gas-phase spectra. Simple physisorption does not affect the analyte IR spectra.

There are three main changes in the spectrum of methyl lactate sorbed by the CD, relative to the PEUT or PIB reference spectra (details of the interpretation of the IR spectra are given elsewhere [41-45]). First, there is a new peak in the OH region around 3470 cm^{-1} (region of intermolecular hydrogen bonds), which is much more pronounced for the R than the S enantiomer, consistent with the longer retention time of the R enantiomer on a GC column [9] and a larger response for this enantiomer from acoustic wave devices (see next section, Figure 6, and Table 1). The peak maximum for the hydrogen bond of the S enantiomer is at 3488 cm^{-1}, that for the R enantiomer is at 3468 cm^{-1}, and the "regular" OH peak is at 3575 cm^{-1}. A similar H-bonding peak occurs for propan-1-ol (not shown) at 3538 cm^{-1} (OH peak at 3672 cm^{-1}) with a lower intensity than either the R or the S enantiomer. Propan-1-ol, however, shows only a slightly increased

partition coefficient with the CD relative to the reference polymers PIB and PEUT (as inferred from TSMR data; see Table 1). Thus, the occurrence of new vibrational peaks suggests a specific interaction (in the case of the methyl lactate enantiomers and propan-1-ol, H-bridging) but does not necessarily imply anomalously high partition coefficients. While the intensity of such peaks may offer a qualitative idea about the strength of the specific interactions, our data do not reveal any simple, direct correlation between the number and/or intensity of these new vibrational bands and the magnitude of the partition coefficient. A comparison of the intensities of spectral changes is likely to be most meaningful in the case of very similar molecules, such as the two optical isomers of methyl lactate.

The positions of the new OH peaks resulting from H-bonding between the CD and the R and S enantiomers of methyl lactate differ by 20 cm^{-1}. Badger *et al.* showed that the magnitude of the shift in the OH fundamental mode due to hydrogen bonding can be used as a measure of the strength of that bond, with a proportionality constant of about 8.5 cm^{-1}/(kJ/mol) [46]. In the case of the two enantiomers, this implies a difference of 2.3 kJ/mol from our IR data, which is comparable to the $\Delta\Delta G$ value (enantiomeric difference in Gibb's free energy of sorption) determined by gas chromatography of 4 kJ/mol. The appearance of the H-bonding band in the IR spectrum, which calculation suggests may account for a substantial fraction of the enantiomeric difference in the free energy of sorption, indicates that the OH group probably contributes to a significant extent to the enantiomeric discrimination process in the case of methyl lactate.

Further spectral changes for methyl lactate include a shoulder in the C=O stretching region at 1725 cm^{-1}, together with a slight change in the peak shape of the C=O peak (intensity increase on the low-energy flank) and a new peak or shoulder in the C–O stretching region at 1190 cm^{-1}. The intensity of these C–O and C=O changes again varies between the R and S enantiomers, the changes in the R-methyl lactate spectrum being the more pronounced, consistent with stronger sorption of the R-enantiomer into the CD matrix [9].

Intriguing results are obtained for an analyte identical to methyl lactate, save for the replacement of the —OH by a —Cl group in the "2" position. The IR spectral changes

associated with the sorption of methyl 2-chloropropionate are shown in Figure 5, from bottom to top: reference polymer spectra (PIB, PEUT, $p/p_0 = 2.7\%$); R enantiomer ($p/p_0 = 2.7\%$); S enantiomer ($p/p_0 = 2.7\%$ and 5%). In contrast to the H-bonding results for methyl lactate, sorption of the two enantiomers of methyl 2-chloropropionate by the CD causes no changes in the carbon–chlorine or H–Cl regions of the IR spectrum, indicating no analogous intermolecular hydrogen bonds. This is not at all surprising, since the CD has no significant H-bond donor sites to interact with the Cl, but nonetheless it may help to explain why there is an inversion in the elution order for GC columns [9], as well as a reversal of the relative acoustic wave sensor signal magnitudes (Figure 6, Table 1), in going from methyl lactate, for which R interacts more strongly than S, to methyl 2-chloropropionate, for which the converse is true [9]. As in the case of the structurally very similar methyl lactate, a shoulder appears on the C=O stretch at 1747 cm^{-1}, for both chloropropionate enantiomers (Figure 5). However, consistent with the inverted enantiomeric preference, this shoulder is more pronounced for the S than the R enantiomer. In addition, Figure 5 shows a remarkable variation in the peak intensity in the C–O stretching region at 1200 cm^{-1} (compared to the neighboring peak at 1179 cm^{-1}), in addition to the disappearance of the shoulder at 1109 cm^{-1} (the C–O stretch of C–OR). The changes in the C=O and C–O regions for both methyl lactate and methyl 2-chloropropionate support our previous speculation that the presence of a methoxy, halogenated methoxy, or ester group promotes preferential sorption in the CD torus [9]. This is believed to be a result of the methoxy functionality being the proper size and shape to fit snugly into the central region of the torus, a hypothesis that is supported by a measured stoichiometry between CD and either of the propionates of approximately 1:1 (in the low-concentration "Langmuirian" sorption regime).

When interpreting the spectral changes for the propionates, one must also take into consideration the fact that the CD itself has a C=O absorbance at 1758 cm^{-1} and a C–O absorbance at 1179 cm^{-1}. Hence, the observed spectral changes associated with those functionalities could arise from a shift of either the bands of the analyte *or* the CD (or perhaps both) due to the specific interactions. However, similar spectral changes have been recorded for the anesthetics enflurane and isoflurane sorbed by the same CD used in

this work [47]. These changes, measured using attenuated total internal reflection IR, affect mainly the C–F bands of the two anesthetics and therefore can be associated only with the analyte molecules, not the CD. This report, coupled with the fact that the CD molecular cage is not particularly rigid and is relatively large compared to the analyte molecular dimensions, allowing minor conformational changes with little energetic penalty, leads us to believe that the C=O and C–O vibrational changes in Figures 4 and 5 are associated with the analytes. In the OH region for methyl lactate, where the unoccupied CD has no IR absorbance, the formation of a lactate—CD intermolecular hydrogen bond results in an absorbance involving both analyte and host.

Another feature of the spectral changes of both propionates interacting with the CD is saturation in absorbance intensity as analyte concentration increases: the new OH peak of methyl lactate, or the C–O stretch change of methyl 2-chloropropionate, for example, has nearly achieved maximum intensity at $p/p_0 = 2.7\%$. Upon increasing the analyte concentration to 5.4% (top spectrum) or 10.8% of saturation (not shown), the "regular" OH peak for methyl lactate at 3575 cm^{-1} gains much more intensity than the shoulder at 3468 cm^{-1}; the same holds true for the changes in the C–O stretching region (1200 cm^{-1} and 1179 cm^{-1}) of methyl 2-chloropropionate. This saturation of the signal, which has been observed by other authors as well [40], results from the limited number of preferential sorption sites available in the coating: the intensity of the changes caused by this preferential sorption attains its maximum when all such sites are occupied. For the propionates interacting with the CD, this occurs near $p/p_0 = 2\%$. From the TSMR investigations, we know that at most 80% of all the cyclodextrin molecules are accessible to the analyte [9].

Finally, we note that no spectral changes were observed for either the analytes or the CD upon coating exposure to *n*-octane, toluene, trichloromethane, or tetrachloroethene. This confirms that spectral perturbation is not invariably associated with sorption of an analyte by the CD, even for cases such as trichloromethane, in which SAW results show a response signal comparable to that for the propionates.

Acoustic wave sensor results. SAW responses recorded concurrently with the IR measurements for the CD and the two reference polymers are summarized in Figure 6 for

exposure to the two propionates (both enantiomers of each) as well as the set of "reference" solvents (*n*-octane, propan-1-ol, toluene, trichloromethane, and tetrachloroethene). The frequency shifts (3 different concentrations per analyte) of each of the three delay lines constituting one of the SAW/IR devices were normalized by dividing by the p/p_0 and molecular weight of the analyte. Normalization for p/p_0 was done over a fairly narrow range of concentrations, where the response was approximately linear with concentration. These responses were further normalized to the magnitude of the response from *n*-octane for each delay line, to compensate for differences in coating thickness among the three delay lines distributed over this relatively large (4 x 1.5 cm) device. Finally, all of the normalized responses for a given analyte were averaged to yield one datum per analyte/coating combination. These average values are characterized by a standard deviation that is some 10 – 20% larger than for "ordinary" SAW delay lines operating at the same frequency (the latter having 230 wavelength IDT spacing rather than 312 for the SAW/IR devices).

SAW devices are subject to modulus and viscosity effects in addition to mass loading [27,28], so deviations from the true thermodynamic ("mass-only") response are possible, particularly for very soft materials (the CD coating on the device has the appearance of an oil). We therefore believe the discrepancies between the average SAW responses in Figure 6 and the "thermodynamically" normalized partition coefficients (normalized analogously to the SAW signals, for details see table caption) from TSMR measurements of the same coating/analyte interactions, reported in Table 1, are partly a result of such viscoelastic nonidealities.

Normalization of sensor signals for analyte vapor pressure (which is typically a good estimate of fugacity, particularly well below saturation) allows thermodynamic comparisons to be drawn between the responses to different analytes, within the limits of any analyte- or concentration-dependent viscoelastic effects. In the event that sensor response depended only upon analyte thermodynamic activity (fugacity), all the responses in Figure 6 would be approximately equivalent, as would all the normalized partition coefficients reported in Table 1. Within a factor of approximately two, such behavior is found for PIB for the analytes octane, toluene, trichloromethane, and

tetrachloroethene for both the SAW (Figure 6) and TSMR (Table 1) responses. For the more polar analytes, the nonpolar PIB has considerably less affinity. For the more polar polymer PEUT, deviations from a pure p/p_0 response are significant for nearly all analytes.

In the event that pronounced molecular recognition leads to anomalously large partition coefficients for some analytes, the corresponding bars in the graph of Figure 6 should stand out from the rest. This seems to be the case for the propionates, although not to the extent expected (compare Table 1). At least part of the reason for this is straightforward: to have enough analyte in the film for measurable spectral changes to be recorded, we found it necessary to use a minimum vapor concentration of about 2% of p/p_0. This, unfortunately, is in the region of the sorption isotherm (Figure 1) where saturation of most of the selective sites has already occurred, and the slope is consequently decreasing; the response in this regime is, in significant measure, Henry's Law behavior. The TSMR partition coefficients in Table 1, however, are determined according to ref. 30 from the initial slope at very low concentrations and therefore show the preferential sorption more dramatically. Both SAW and TSMR [9] sensor results show a clear discrimination of the enantiomers (signal intensity variations are consistent with elution order in GC) of both pairs of the propionates. Both sensor platforms also show large responses to trichloromethane. Besides the different concentration ranges used for the determination of the SAW and TSMR response (p/p_0 at least 2 - 5% for the FTIR/SAW, but below 0.2% for the TSMR), further relative discrepancies between SAW and TSMR results are probably due in significant measure to the fact that SAW responses are, for some materials in some thickness ranges, significantly more sensitive to viscosity and modulus effects.

π-Stacking: Ni Phthalocyanine

Here, chemical specificity is expected to result from an intense interaction of the large, delocalized π-electron system of the phthalocyanine with easily polarizable electron systems (bromine, iodine, etc.), with unsaturated π-bonded compounds (alkenes, etc.), and the strongest interactions are expected with π-electron-containing aromatic ring

compounds. In brief, for all π-system compounds examined (particularly the four aromatic ring compounds), we find clear changes in the IR signature of the PC, along with enhanced partition coefficients and SAW responses, indicative of specific chemical interactions. No spectral changes occur when the π analytes are sorbed by the conventional "reference" polymers, nor for exposure of NiPC to *n*-octane, propan-1-ol, or trichloromethane.

FTIR-ERS results. Figure 7 shows, from bottom to top, the spectra of tetrachloroethene sorbed in PEUT and NiPC ($p/p_0 = 5.8\%$), the reflection absorption spectrum of the pure NiPC, and the spectra of benzene in NiPC and PEUT ($p/p_0 = 3.1\%$). Figure 8 shows the spectra of toluene: $p/p_0 = 1.2\%$ and 3% in NiPC, as well as $p/p_0 = 1.2\%$ in PIB and PEUT. Again, the spectra recorded for the PEUT and PIB coatings are identical to those of the pure solvent vapor. The most obvious changes in the spectra when comparing PIB or PEUT to NiPC are a number of "negative" peaks arising at frequencies characteristic of the NiPC absorbance spectrum (shown in Figure 7; the spectra of most metal phthalocyaninato complexes are very similar. See, e.g., refs. 48 and 49). This is most clear in the case of tetrachloroethene (Figure 7), which has no characteristic absorbance in this (aromatic) spectral region, but also occurs in the case of benzene.

There are several possible explanations for the decrease in intensity of the NiPC peaks upon exposure to the analyte vapor. One is that the effective optical path through the NiPC film decreases as a consequence of a change in the refractive index, which could result from a perturbation of the NiPC's electronic structure, particularly that associated with the aromatic structure, by the π-stacking process. The NiPC, as well as the Ni camphorate (discussed below), are deposited as polycrystalline thin films. It is possible, therefore, that insertion of π-stacking analytes between adjacent phthalocyanines could affect the morphology or packing of the crystallites, thereby altering the optical parameters [50]. It is significant that we observed no comparable effects in the case of any of the polymers or the "oily" CD layer; only the polycrystalline materials show such effects. No such negative peaks were observed as a result of the sorption of *n*-octane, trichloromethane, or propan-1-ol.

For the unsaturated compound with the smallest π system of those examined, tetrachloroethene, the negative peaks are relatively weak, as shown in Figure 7. Besides the small negative NiPC peaks, the other spectral changes associated with the sorption of tetrachloroethene by NiPC are a small positive peak at 1095 cm^{-1}, and the absence of a negative peak at 1391 cm^{-1} (discussed in the next paragraph).

For benzene (Figure 7), toluene (Figure 8), *m*-xylene, and pyridine, the negative peaks resulting from sorption by the NiPC have considerable intensity. It is remarkable that the NiPC peak at 1391 cm^{-1} (associated with C–H deformations) does not occur as a negative peak; the reason for this is not clear. For all four aromatic compounds, as well as tetrachloroethene, a characteristic peak appears at 1095 cm^{-1} (Figure 7, Figure 8). Since this peak has precisely the same frequency for all five π compounds, it probably originates from the phthalocyanine (in contrast to the situation described above for the CD, where the spectral changes were all associated with the analytes). In the absence of analyte, the NiPC, has a set of bands at 1065 cm^{-1} and 1105 cm^{-1} (Figure 7), which are characteristic of the metal coordination state [49]. It seems likely, therefore, that upon adsorption to the NiPC system, the aromatics either (partially) occupy the free coordination sites of the metal (the NiPC complex is planar) or influence the PC donor bonds to the metal. Further evidence for the important role of the metal is provided by the fact that the sensor responses of the phthalocyanines drastically decrease when two axial ligands are introduced, or no metal central atom (2 H atoms instead) is present [16]. Unfortunately, the reflection IR technique does not allow the study of the 500 – 100 cm^{-1} region, where the ring deformation bands of the phthalocyanine and the $M–N_4$ stretching bands are located [53].

Another significant spectral change occurs in the ring-breathing-mode region of benzene, toluene, and *m*-xylene. A shoulder appears on the high-energy flank of the ring-breathing peak at 1530 cm^{-1} for benzene (Figure 7), and at 1528 cm^{-1} for toluene (Figure 8) and *m*-xylene (not shown). The symmetry of this ring-breathing peak is clearly altered, but in the case of benzene this might result from superposition of this peak (1484 cm^{-1}) with the negative peaks discussed above (see Figure 7). In the case of toluene (Figure 8) and *m*-xylene (not shown), the ring-breathing modes are shifted to somewhat

higher frequency (1501 cm^{-1}) and, hence, there is no interference from the negative peaks. Also for toluene and *m*-xylene, we observe changes in the peak shape (dips) of the out-of-plane deformation of ring H-atoms; these very intense peaks are located at 729 cm^{-1} for toluene and 770 cm^{-1} for *m*-xylene.

Acoustic wave device results. Consistent with the smaller spectral changes compared to benzene, toluene, *m*-xylene, and pyridine, the tetrachloroethene sorption isotherm is linear and the partition coefficients are not nearly as large as those of the aromatic ring compounds (Figure 9, Table 2). In contrast, the four aromatic ring compounds exhibit nonlinear sorption characteristics and significantly increased partitioning in the Ni-phthalocyanine matrix (Figure 9, Table 2). The bars representing the NiPC-coated SAW-device responses to the aromatics stand out markedly in Figure 9. The large response to trichloromethane might be a result of interactions between the PC π cloud and the somewhat acidic proton on trichloromethane.

The sensor response from a NiPC-coated TSMR, upon exposure to toluene, is shown in Figure 10. Although the coating material is polycrystalline, the sensor response is rapid and a stable equilibrium state is reached quickly at each concentration. The low noise of the sensor signal and the stability of the baseline are also notable in Figure 10. The response as a function of concentration is clearly nonlinear (as in the isotherms for the CD in Figure 1), consistent with a dual-mode sorption process, characteristic of specific chemical interactions, as discussed in the previous section. The possibility of modeling and fitting such responses was discussed above in the context of the CD and in detail in ref. 9.

Metal coordination: Ni camphorate

Due to the nature of coordinative ligand–metal donor bonds, the spectral changes are expected to be more pronounced for the transition metal camphorate complex (see Figure 2) than in the case of the CD and the NiPC. Note that the two water ligands are weakly bound, so this complex is effectively coordinatively unsaturated, and therefore readily binds Lewis bases. Earlier TSMR investigations revealed fully reversible but slow sensor response characteristics, along with a significantly enhanced interaction energy relative to

conventional polymers [15]; the enrichment of the analyte in the bulk coating material is therefore expected to be relatively high. Since the Ni-camphorate is polycrystalline like the NiPC, the same considerations discussed in the previous section hold for the "negative" spectral peaks associated with Ni-Cam upon sorption of some analytes. Fortunately, the Ni-Cam has only a few absorbances of low intensity in the spectral regions of interest, as detailed below.

FTIR-ERS results. Dimethylmethylphosphonate (DMMP) was selected as an oxygen-containing σ-donor ligand. Figure 11 shows the spectra of $p/p_0 = 5.5\%$ DMMP in PIB, PEUT (*p*-polarized spectra, which are identical to the gas-phase spectra), as well as the *s* and *p* spectra for DMMP sorbed by Ni-Cam. As expected, the spectral changes are more intense in the surface-sensitive *p*-polarized spectrum. The enhanced sorption (peak intensity) in the Ni-Cam, as compared to the reference polymers, is apparent. In addition to an appreciable increase in the intensity of most of the peaks and a few "negative" peaks (marked with asterisks), there are three major changes in the spectra. From left to right, the first significant change occurs in the C=O region. Ni-Cam has a C=O absorbance at 1640 cm^{-1}. A large "dip" is recorded at 1636 cm^{-1}, and two new peaks appear at 1650 and 1665 cm^{-1}. The dip may be partially attributable to a negative peak, but compared to the intensity of the other negative peaks, it is probable that there are additional structural changes responsible for this change: the β-diketonate coordination to the Ni appears to undergo changes upon coordination of the phosphonate to the Ni. The β-diketonate and Ni form a delocalized π-system (β-diketonate acts as a σ electron donor and π acceptor for the coordinative bonds) [15]. Upon coordination of the phosphonate ligand, the Ni receives additional σ electron density from this new donor, but probably also back-donates to the P=O π system, hence reducing the electron density that is back-donated to the C=O π bonds. Because the C=O π bonds are predominantly antibonding in character, diminishing the back donation into these bonds enhances the overall strength of the C=O bond, shifting it to higher energy (wavenumber) [54]. This, we believe, is responsible for the two new bands at 1650 and 1665 cm^{-1}, in addition to and contributing to the dip at 1636 cm^{-1}. (For comparison, the C=O bands of the uncoordinated free camphorate are at 1700 cm^{-1}).

Related to the change in the C=O bands is the appearance of a peak at 1529 cm^{-1}. This peak also can be attributed to changes in the β-diketonate–Ni system: it is characteristic of the combination of C=O and C=C in the aromatic system of the Ni-Cam [45,55]. The increased intensity of this peak indicates changes in this aromatic system. Both the changes in the C=O region and the peak at 1529 cm^{-1} are characteristic of the camphorate and should occur upon exposure to any specifically-recognized analyte (compare Figure 12 for a nonspecific analyte, as discussed below).

The third set of obvious changes is related to the phosphonate analyte. The P=O stretch at 1276 cm^{-1} maintains its intensity when comparing PIB or PEUT (equivalent to gas-phase DMMP spectra) to the *s* and *p* spectra of the camphorate. This band is therefore assigned to the P=O stretch of the free vapor-phase molecule, since the gas-phase concentration is identical for all coatings. Near this peak, however, there arises a new peak at 1247 cm^{-1}, also in the P=O region, and only for the Ni-Cam coating, due to the Ni-coordinated phosphonate. This bathochromic shift of nearly 30 cm^{-1} relative to the free phosphonate supports the hypothesis presented above in the discussion of the C=O band shift, namely that some of the Ni π electron density is back-donated to the antibonding π levels of the P=O bond, weakening it, but strengthening the C=O bond as a result. The appearance of the weakened P=O band at 1247 cm^{-1} suggests significant interaction between Ni and the phosphoryl oxygen. In addition, there are several minor spectral changes in the phosphonate spectrum: the P–CH_3 symmetric deformation at 1314 cm^{-1} increases in intensity, the asymmetric P–O–C stretch is slightly shifted from 1052 to 1045 cm^{-1}, the symmetric P–O–C stretch is slightly shifted from 819 to 828 cm^{-1}, and the P–CH_3 rock at 920 cm^{-1} develops a new shoulder. All these peaks gain intensity, since the positions of the original gas-phase peak and the peak of the absorbed species are at the same or very similar frequencies. The only gas-phase peak that differs in frequency from the adsorbed species enough that it gains no intensity is the P=O peak at 1276 cm^{-1}.

We note that the affinity of DMMP for this coordinatively unsaturated Ni complex has parallels to our work on the selective detection of a closely related organophosphonate, diisopropylmethylphosphonate (DIMP). In the case of DIMP, we found that self-assembled monolayers terminated by coordinately unsaturated copper

resulted in selective binding of DIMP relative to a range of organic compounds, using the SAW platform [17,56]. Further, an extensive IR reflectance study revealed similar effects on the bands characteristic of the phosphonate upon reversible coordination of the DIMP [57].

The spectra associated with the sorption of a nitrogen-containing aromatic compound, pyridine, are shown in Figure 12. The *p*-polarized spectra of PIB and PEUT upon exposure to 2.9%-of-saturation pyridine and the *p* spectra of Ni-Cam upon exposure to 1.1 and 2.9% pyridine are depicted. It is notable that the enrichment of the analyte (as indicated by the analyte IR peak intensity) in the coating is not as pronounced as in the case of DMMP. This is due to the higher saturation vapor pressure of pyridine as compared to DMMP. Again, spectral changes related to the camphorate are observed: a dip at 1626 cm^{-1} and two new peaks at 1647 and 1661 cm^{-1} in the C=O region, and a new peak in the region of the aromatic Ni-β-diketonate system at 1527 cm^{-1}. In analogy to the situation described above for the phosphonate and Ni-Cam, the appearance of the two C=O peaks at higher energy is consistent with the π system of the pyridine accepting π back-donation from the Ni, lessening the amount of donation to the antibonding C=O π system, thereby strengthening that bond.

The gas-phase (or PIB or PEUT) spectrum shows mainly a doublet at 1588 and 1577 cm^{-1}, as well as a double peak at 1448 and 1436 cm^{-1}, all of which can be assigned to ring-breathing modes of the pyridine. In the Ni-Cam spectra, the symmetry of the 1448/1436 cm^{-1} pyridine double peak is clearly altered, the high-frequency peak at 1450 cm^{-1} having a marked increase in intensity. In the 1.1% Ni-Cam spectrum, these changes are even more obvious, since the gas-phase signals are still comparably small. As the analyte concentration increases from 1.1 to 2.9%, the right side of the double peak increases to somewhat more than in the gas-phase or reference polymers, while the peak at 1450 cm^{-1} grows only slightly. The other changes occur in the 1577/1588 cm^{-1} doublet. The peak at 1577 cm^{-1} is intensified, thus changing the symmetry of the doublet, and a new peak at 1605 cm^{-1} appears clearly in the 1.1% spectrum. Increasing the gas-phase concentration of pyridine from 1.1 to 2.9% causes the intensity of the gas-phase peaks (1588 and 1577 cm^{-1}) to increase correspondingly. The changed symmetry and the new peak remain

visible, although their intensity increases no further. The changes in this spectral region upon increasing the pyridine concentration from 1.1 to 2.9% are reminiscent of the saturation behavior discussed above for the CD coating: as soon as the preferential sorption sites have been occupied, the intensity of the spectral changes due to preferential sorption increases no further. The concentration limit at which such saturation effects occur depends strongly upon the vapor pressure of the analyte and the site/analyte interaction energy.

The changes in the region of the ring-breathing modes indicate that the symmetry and the electron-density distribution of the aromatic ring system change upon coordination of the N atom to the Ni. Further changes occur in the region of the out-of-plane C–H deformations (745 cm^{-1}) and the ring deformations (701 cm^{-1}). In addition, two new satellite peaks appear at 758 and 632 cm^{-1}, and the shape of the ring-deformation peak at 701 cm^{-1} changes, giving further indication of changes in the ring-breathing region.

For *n*-butylamine (spectra not shown), we find, in addition to the changes related to the camphorate, changes in the NH_2 stretching and wagging regions: a new peak appears at 3280 cm^{-1}, shifted to lower frequency relative to the original NH_2 stretch of the gas-phase molecule at 3347 cm^{-1}, and a shoulder appears at 739 cm^{-1} on the low-energy flank of the NH_2-wag at 780 cm^{-1}. The new NH_2 stretching peak is close to that of a secondary amine, consistent with coordination of the primary amine group to the Ni; the same holds for the shoulder on the NH_2 wag. A similar shift can be observed for the C–N stretch: a new peak occurs at 1023 cm^{-1}, shifted from the 1088 cm^{-1} C–N stretch observed in the gas-phase (or PIB) spectrum.

The weakly coordinating oxygen-containing compounds propan-1-ol and THF show the changes in the spectral bands of the camphorate, but no other changes; coordination may be too weak to affect the spectra of these ligands. No changes at all were observed upon exposure to toluene, octane, tetrachloroethene, trichloromethane, and, perhaps surprisingly, pyrrole.

The spectra of pyrrole (gas, sorbed in PIB, sorbed in Ni-Cam; $p/p_0 = 5.3\%$) are shown in Figure 13. There are no spectral changes relative to the gas-phase spectrum for

either coating. The series of closely-spaced peaks in the 1800 – 1500 cm^{-1} region result from water absorbed into the vapor source (a gas washing bottle). Pyrrole has a nitrogen atom and is heteroaromatic; the free electron pair of the nitrogen is part of the aromatic system; therefore, the Lewis basicity of the N, and hence its ability to donate electrons into a coordinative bond with the Ni-atom, are quite low (there is even a positive dipole charge on the N-atom) : pyrrole is a very poor electron donor or ligand.

Acoustic wave device results . The acoustic wave sensor data, presented in Figure 14 and Table 3, are consistent with the IR results discussed above. Large increases in the sensor signals were recorded for the weakly coordinating oxygen-containing compounds THF and DMMP, with fairly remarkable enhancement of the signal for the nitrogen-containing compounds pyridine and *n*-butylamine, both good Lewis bases. Consistent with the absence of any spectral changes in the case of pyrrole, neither the sensor signals (Figure 14, Table 3) nor the GC retention time for this molecule are enhanced in comparison to the reference polymers [15]. Again, the occurrence of spectral changes is closely correlated to anomalously high partition coefficients.

CONCLUSIONS

The method of simultaneous SAW/*in-situ* FTIR measurements is an effective, powerful tool for elucidating interactions between coatings and gaseous analytes, providing direct evidence for specific interactions between volatile analytes and coating materials on acoustic wave gas sensors. Our SAW/FTIR results support earlier conclusions derived from TSMR data [9,15,16] regarding molecular specificity of several thin-film materials. In most cases where specific chemical interactions—here including metal coordination, cage-compound formation, and π stacking—are expected, we record distinctive, assignable changes in the IR spectra, together with anomalously large SAW sensor responses, upon analyte dosing. It is interesting to note that the spectral changes associated with molecular recognition affect mainly the spectral bands of the analytes in the case of the toroidal cyclodextrin, however, the spectral bands of both the coating material and the analyte in the case of the delocalized π system-containing phthalocyanine as well as in the case of the Ni camphorate coordination complex.

In contrast, for ordinary physisorption processes, exemplified by the conventional organic polymers PEUT and PIB interacting with various volatile organic compounds, no changes in the IR spectra occur either for analytes or coatings, and SAW responses are smaller. For those conventional polymers, the partition coefficients [9] tend roughly to follow the fraction of saturation vapor pressure, although significant variations occur, particularly when comparing the nonpolar poly(isobutene) to the polar poly(etherurethane).

From the results presented in this paper, we conclude that the process of "molecular recognition" in chemical sensors, although it has been a source of some controversy in the literature, is generally viable. However, there are some important factors to take into account; their neglect may have contributed to the debate on this issue. First, in the context of reversible sorption-based gas sensors, molecular recognition should not be viewed as a general means to obtain selectivity ratios of many orders of magnitude for one compound or chemical class relative to chemically similar interferents. Rather, molecular recognition strategies will be most often successful when applied in one of two scenarios. If the single species or family to be detected is chemically very different from the probable interferents (and these interferents occur at p/p_0 levels comparable to, or less than, the analytes), then the attainable selectivity ratios of hundreds to thousands will often suffice.

In a more general approach, which can be applied to the recognition of chemically similar species or families, and even the detection of a low concentration of analyte in a more concentrated interferent background, molecular recognition materials can be used as one or more of the elements in a chemical sensor array. The molecular recognition material can provide the "dominant" response axis for a target analyte, but when the array is comprised of a number of chemically diverse elements, the overall response pattern compensates for poor selectivity ratios and nonspecific responses from high-concentration interferents. The molecular recognition/array strategy is particularly powerful because it allows the rapid and deliberate selection of array elements based upon established interaction chemistries.

The results of the present work lead to one other critical consideration for the application of molecularly selective materials: with few exceptions, enhanced selectivity effects occur at low analyte concentrations. The definition of "low" concentration depends upon the interaction energy for a particular analyte/coating pair, but for the materials and chemicals we have reported on here, it typically occurs for p/p_0 levels below 1 - 2%. At high analyte concentrations, nonspecific physical sorption will invariably dominate. Chemical sensor array systems designed to use molecular-recognition materials, with full awareness of their limitations, should be very effective.

ACKNOWLEDGMENTS

The authors thank Prof. V. Schurig, (Institute of Organic Chemistry, University of Tübingen) for providing the modified cyclodextrin and the Ni-camphorate, and M. Hees and Prof. M. Hanack (Institute of Organic Chemistry, University of Tübingen) for providing the Ni-phthalocyanine. Additionally, we thank C. Fietzek (Institute of Physical Chemistry, University of Tübingen) for determining some of the partition coefficients. We gratefully acknowledge the excellent technical assistance of A. W. Staton (Sandia National Laboratories) with SAW measurements and the measurement cell design and fabrication. We acknowledge many helpful technical discussions with Li Sun and Prof. R. M. Crooks (Dept. of Chemistry, Texas A&M University). R. M Crooks played a key role in conceiving our particular version of the combined SAW/FTIR measurement system. Finally, we owe a debt of gratitude to Dr. Ross C. Thomas (Eltron, Inc.; formerly of Sandia National Laboratories), who led the design and setup of our SAW/FTIR measurement system, and demonstrated its viability. Sandia is a multiprogram laboratory operated by Sandia Corporation, a Lockheed Martin Company, for the United States Department of Energy under Contract DE-AC04-94AL85000.

REFERENCES

1. Carey, W. P.; Beebe, K. R.; Kowalski, B. R. *Anal. Chem.* **1986**, *58* , 149-153.
2. Ballantine, D. S.; Rose, S. L.; Grate, J. W.; Wohltjen, H. *Anal. Chem.* **1986**, *58*, 3058-3066.
3. Osbourn, G. C.; Bartholomew, J. W.; Ricco, A. J.; Crooks, R. M. *Acc. Chem. Res.* **1998**, *31*, 297; Ricco, A. J.; Crooks, R. M.; Osbourn, G. C. *Acc. Chem. Res.* **1998**, *31*, 289.
4. Hierlemann, A.; Schweizer-Berberich, M.; Weimar, U.; Kraus, G.; Pfau, A.; Göpel, W. *Pattern Recognition and Multicomponent Analysis*. in *Sensors Update*; Baltes, H.; Göpel, W.; Hesse, J., Eds.; VCH: Weinheim, Germany, 1996.
5. Lehn, J. M. *Angew. Chem., Int. Ed. Engl.* **1988**, *27*, 89-112.
6. Lehn, J. M. *Science* **1985**, *227*, 849.
7. Rebek, J. *Science* **1987**, *235*, 1478-1484.
8. Bodenhöfer, K.; Hierlemann, A.; Seemann, J.; Gauglitz, G.; Christian, B.; Koppenhoefer, B.; Göpel, W. *Nature* **1997**, *387*, 577 and *Anal. Chem.* **1997**, *69*, 3058-3068.
9. Bodenhöfer, K.; Hierlemann, A.; Juza, M.; Schurig, V.; Göpel, W. *Anal. Chem.* **1997**, *69*, 4017-4031.
10. Dickert, F. L.; Bruckdorfer, T.; Feigl, H.; Haunschild, A.; Kuschow, V.; Obermeier, E.; Bulst, W.; Knauer, U.; Mages, G. *Sens. Actuators* B **1993**, *13-14*, 297-301.
11. Dickert, F. L.; Haunschild, A. *Adv. Materials* **1993**, *5*, 887-895.
12. Schierbaum, K. D.; Weiss, T.; Thoden van Velzen, E.U.; Engbersen, J. R.; Reinhoudt, D. N.; Göpel, W. *Science*, **1994**, *265*, 1413-1415.
13. Nelli, P.; Dalcanale, E.; Faglia, G.; Sberveglieri, G.; Soncini, P. *Sens. Actuators B* **1993**, *13-14*, 302-304.
14. Grate, J. W.; Patrash, S. J.; Abraham, M. *Anal. Chem.*. **1996**, *68*, 913.
15. Hierlemann, A.; Bodenhöfer, K.; Fluck, M.; Schurig, V.; Göpel, W. *Anal. Chim. Acta* **1997**, *346*, 327.
16. Fietzek, C.; Bodenhöfer, K.; Hees, M.; Haisch, P.; Hanack, M.; Göpel, W. *Proc. Eurosensors 1998*, Southhampton, England, manuscript in preparation.

17. Thomas, R. C.; Yang, H. C.; DiRubio, C. R.; Ricco, A. J.; Crooks, R. M. *Langmuir* **1996**, *12*, 726.

18. Greenler, R. G. *J. Chem. Phys.* **1966**, *44*, 310.

19. Ferraro, J. R.; Basile, L. J. *Fourier transform Infrared Spectroscopy*; Academic Press: New York, 1985; Chapters 7-8.

20. Yates, Jr., J. T.; Madey, T. E. *Vibrational Spectroscopy of Molecules on Surfaces*; Plenum Press: New York, 1987; Chapter 7.

21. Bubeck, C.; Holtkamp, D. *Adv. Mater.* **1991**, *3*, 32.

22. Porter, M. D. *Anal. Chem.* **1988**, *60*, 1143A.

23. Crooks, R. M.; Sun, L.; Xu, C.; Hill, S. L.; Ricco, A. J. *Spectroscopy* **1993**, *8*, 28.

24. Greenler, R. G. *J. Vac. Sci. Technol.* **1975**, *12*, 1410.

25. Corn, R. private communication.

26. Thomas. R. C.; Hierlemann, A.; Staton, A. W.; Hill, M.; Ricco, A. J. manuscript in preparation.

27. *Acoustic Wave Sensors: Theory, Design, and Physico-Chemical Applications*; D. S. Ballantine, R. M. White, S. J. Martin, A. J. Ricco, G. C. Frye, E. T. Zellers, and H. Wohltjen, Academic Press: San Diego, 1997.

28. Martin, S. J.; Frye, G. C.; Senturia, S. D. *Anal. Chem.* **1994**, *66* , 2201.

29. Sauerbrey, G. *Z. Phys.* **1959**, *155*, 206-222.

30. Bodenhöfer, K.; Hierlemann, A.; Noetzel, G.; Weimar, U.; Göpel, W. *Anal. Chem.*, **1996**, *68*, 2210.

31. Grate, J. W.; Martin, S. J.; White, R. M. *Anal. Chem.* **1993**, *65*, 940A-948A and 987A-996A.

32. Nieuwenhuizen, M. S.; Venema, A. *Sens. Mater.* **1989**, *5*, 261-300.

33. König, W. A.; Krebber, R.; Mischnick, P. *J. High Resolut. Chromatogr.* **1989**, *11*, 732-738.

34. Haisch, P.; Hanack, M. *Synthesis* **1995**, *19*, 1251.

35. Bodenhöfer, K.; Hierlemann, A.; Schlunk, R.; Göpel, W. *Sens. Actuators B* **1997**, *45*, 259-264.

36. Riddick, J. A.; Bunger, W. B.; Sakano, T. K. Organic Solvents. In *Techniques of Chemistry*; Weissberger, A. Ed.; Wiley Interscience: New York, 1986; Vol. II.

37. Ricco, A.J.; Frye, G.C.; Martin, S.J. *Langmuir* **1989**,*5*, 273.

38. Thomas, R. C.; Sun, L.; Crooks, R. M.; Ricco, A. J. *Langmuir* **1991**, *7*, 620.

39. Rodgers, C. E. In *Polymer Permeability*; Comyn, J., Ed.; Elsevier: New York, 1985, pp. 29-34.

40. Dickert, F. L.; Haunschild, A.; Kuschow, V.; Reif, M.; Stathopulos, H. *Anal. Chem.* **1996**, *68*, 1058-1061.

41. Fateley, W. G.; Dollish, F. R.; McDevitt, N. T.; Freeman, F. B. *Infrared and Raman Selection Rules for Molecular and Lattice Vibrations*; Wiley Interscience: New York, 1972.

42. Bellamy, L. J. *Advances in Infrared Group Frequencies*; Methuen: London, 1958.

43. Bellamy, L. J. *The Infrared Spectra of Complex Molecules*; Chapman and Hall: London, 1980.

44. Colthup, N. B.; Daly, L. H.; Wiberley, S. E. *Introduction to Infrared and Raman Spectroscopy*; Academic Press: San Diego, 1990.

45. Nakamoto, K. *Infrared and Raman Spectra of Inorganic and Coordination Compounds, Parts A and B*; Wiley Interscience: New York, 1997.

46. Badger, R. M.; Bauer, S. H. *J. Chem. Phys.* **1937**, *5*, 839.

47. Cramer, M. Ph.D. Dissertation, University of Tübingen, 1997.

48. Kalz, W.; Homborg, H. *Z. Naturforsch.* **1983**, *38b*, 470.

49. Sievertsen, S.; Schlehahn, H.; Homborg, H. *Z. anorg. allg. Chem.* **1993**, *619*, 1064-1072.

50. A less likely explanation also derives from the polycrystalline structure of the NiPC and Ni camphorate. Since polycrystalline materials are densely packed in the crystalline domains, insertion of the analyte molecules into those domains could actually reduce the physical density of the coatings in the near-surface region probed with enhanced sensitivity by the *p*-polarized IR beam; consequently, negative peaks could occur. (In contrast, the polymers and the CD have considerable free volume and should not be similarly affected.) In every case where this effect was observed,

the negative peaks, along with any other spectral changes, are much less pronounced in the *s*- than the *p*-polarized spectrum. Since the reflective layer is gold, since the negative peaks are attributable to simple decreases in absorbances of the coating materials and do not show derivative-like characteristics, and since the *p* and *s* spectra show the same alterations (no ordering effects), we believe that the distortion of spectral bandshapes by optical effects and related phenomena (see refs. 22,51,52) need *not* be taken into account here.

51. Porter, M. D.; Karweik, D.; Kuwana, T.; Theis, W.; Norris, G. B.; Tiernan, T. O. *Appl. Spectrosc.* **1984**, *38*, 11-16.

52. Schlotter, N. E.; Porter, M. D.; Bright, T. B.; Allara, D. L. *Chem. Phys. Lett.* **1986**, *132*, 93-98.

53. Terzian, G.; Moubaraki, B.; Mossoyan-Deneux, M.; Benlian, D. *Spectrochimica Acta* **1989**, *45A*, 675-677.

54. Avanzino, S. C.; Bakke, A. A.; Chen, H.-W.; Donahue, C. J.; Jolly, W. L.; Lee, T. H.; Ricco, A. J. *Inorg. Chem.* **1980**, *19*, 1931.

55. Mikami, M.; Nakagawa, I.; Shimanouchi, T. *Spectrochim. Acta* **1967**, *23A*, 1037.

56. Kepley, L. J.; Crooks, R. M.; Ricco, A. J. *Anal. Chem.* **1992**, *64*, 3191.

57. Crooks, R.M.; Yang, H. C.; McEllistrem, L. J.; Thomas, R. C; Ricco, A. J. *Faraday Discuss.* **1997**, *107*, 285.

Figure captions

Figure 1. Response of two thickness-shear mode resonators as a function of the concentrations of R- and S-methyl lactate (methyl 2-hydroxypropionate). The response of the sensor coated with the chemically nonspecific material polyetherurethane (PEUT; indicated by "–" and "x" for the R and S enantiomers, respectively) is very linear up to 2500 μg/L ($p/p_0 = 7\%$), with a zero intercept, consistent with Henry's Law (simple physisorptive) behavior; there is no measurable difference between the two propionate enantiomers for the PEUT coating. The "bent" isotherms were recorded for a coating of a modified γ cyclodextrin supported in a matrix of poly(dimethylsiloxane) (50% w/w CD in SE 54; indicated by open and filled squares for the R and S enantiomers, respectively). The response from this enantiomerically specific coating is characterized by a Langmuir-like region at low concentrations (up to ~750 μg/L, or $p/p_0 = 2\%$), giving way to linear, physisorptive behavior once all the specific interaction sites (the CD tori in this case) have been filled.

Figure 2. Three molecular-recognition coating materials used to obtain the results from acoustic wave devices and reflection FTIR in this study. The cyclodextrin forms inclusion complexes with appropriately sized analytes bearing suitable functional groups, as described in the text; the Ni camphorate, with two weakly coordinated, readily-displaced water ligands, coordinates a range of Lewis basic ligands, with preference for amines; and the Ni phthalocyanine forms π-stacked composites with analytes having delocalized π systems, particularly aromatic ring structures.

Figure 3. Test fixture and optical setup used to perform simultaneous SAW/*in-situ* FTIR external reflectance measurements. The source and detector are part of a commercial FTIR instrument, the polarizer is a manually rotated wire-grid type,

and a "seagull" reflection accessory (not shown) is used to provide and collect light at an angle of about 80° off normal. Three of the five SAW delay lines (ST-cut quartz; 97 MHz) are electrically connected to make multiple measurements of coating/analyte interactions occurring in the central region of the device; the selective coating is applied on top of the reflective Au layer, which is roughly 8.5 x 40 mm in area.

Figure 4. IR reflectance spectra of: different concentrations of R-methyl lactate (p/p_0 = 5.4 and 2.7% at 30 °C) interacting with a modified γ cyclodextrin (CD), labeled CD R 5 and CD R 3, respectively; S-methyl lactate (p/p_0 = 2.7%) interacting with the CD, labeled CD S 3; and methyl lactate (p/p_0 = 2.7%; no measurable difference between R and S enantiomers) sorbed by the conventional polymers polyetherurethane and polyisobutylene, labeled PEUT and PIB. All spectra were obtained using *p*-polarized illumination, and have the spectrum of the analyte-free coating material subtracted out as background, so that only the spectral bands of the analyte, or those that arise from sorption-induced changes in the coating material, appear in the figure. Spectral changes indicative of specific chemical interactions are marked by pointers and discussed in the text.

Figure 5. IR reflectance spectra of: different concentrations of methyl 2-S-chloropropionate (p/p_0 = 5.4 and 2.7%) interacting with CD, labeled CD S 5 and CD S 3; methyl 2-R-chloropropionate (p/p_0 = 2.7%) interacting with CD, labeled CD R 3; and methyl 2-chloropropionate (p/p_0 = 2.7%; no difference between enantiomers) sorbed by PEUT and PIB. Spectra are *p* polarized and the unperturbed coating spectrum has been subtracted out. Key spectral changes, marked by pointers, are discussed in the text.

Figure 6. Normalized sensor responses upon exposure to a range of analytes of 97-MHz SAW devices incorporated in the reflectance IR substrate (see Figure 3), coated with the selective cage compound CD (Figure 2), as well as conventional

polymers PIB and PEUT. The frequency shifts (three concentrations per analyte, lying in the range $p/p_0 = 2.7 - 5.4\%$) from each of three delay lines were normalized for analyte p/p_0 and molecular weight, then further normalized to the *n*-octane response for the particular delay line to correct for differences in coating thickness. The three normalized responses per coating/analyte combination were averaged to give the bars shown in the figure. Note the preference for the S enantiomer of methyl 2-chloropropionate over the R, and the converse preference for the enantiomers of methyl lactate.

Figure 7. IR reflectance spectra of: benzene (p/p_0 = 3.1%) sorbed by PEUT and interacting with a Ni phthalocyanine (NiPC, Figure 2), labeled BZ/PEUT and BZ/PC; analyte-free NiPC coating, labeled PC; and tetrachloroethene (p/p_0 = 5.8%) interacting with NiPC and sorbed by the conventional polymer PEUT, labeled PCE/PC and PCE/PEUT. With the exception of the pure NiPC coating spectrum, these *p*-polarized spectra have the unperturbed coating spectrum subtracted out. Key spectral changes, marked by pointers, are discussed in the text. The negative peaks in the BZ/PC and PCE/PC spectra correspond to absorbance bands of the NiPC, indicating that sorption of these analytes diminishes the absorbance of the PC at those frequencies.

Figure 8. IR reflectance spectra of: toluene (p/p_0 = 3%) sorbed by the conventional polymers PEUT and PIB (so labeled); and two concentrations of toluene interacting with the NiPC (p/p_0 = 3 and 1.2%), labeled PC 3 and PC 1, respectively. Spectra are *p* polarized and the unperturbed coating spectrum has been subtracted out. Key spectral changes, marked by pointers, are discussed in the text. The negative peaks in the toluene/PC spectra indicate that sorption of this analyte diminishes the absorbance of the NiPC at those frequencies.

Figure 9. Normalized sensor responses upon exposure to a range of analytes of 97-MHz SAW devices incorporated in the reflectance IR substrate, coated with the selective π-stacking material NiPC (Figure 2), as well as the conventional

polymers PIB and PEUT. Three responses per analyte were normalized to p/p_0, molecular weight, and the response to *n*-octane, then averaged, as detailed in the Figure 6 caption. Note the marked preference for the aromatic ring compounds benzene, toluene, and pyridine.

Figure 10. Response from a 30-MHz TSMR [8] coated with NiPC upon exposure to a series of toluene concentration steps; the maximum concentration examined, 600 ppm by volume, is equivalent to p/p_0 = 1.2%. The dotted line marks a hypothetical linear correlation between concentration and frequency shift, based upon the response to the lowest concentration (100 ppm, or p/p_0 = 0.2%); the sublinear response at high concentrations is consistent with dual-mode sorption such as that shown by the isotherms for the CD in Figure 1.

Figure 11. IR reflectance spectra of dimethylmethylphosphonate (DMMP; p/p_0 = 5.5%) interacting with the Ni –camphorate complex depicted in Figure 2, probed with both *p*- and *s*-polarized light (labeled Ni-Cam P and Ni-Cam S, respectively). Clearly, the surface-selection rule leads to significantly more intense sorption-induced changes in the *p* spectrum than the *s*. Also shown are the *p*-polarized spectra for 5.5% DMMP sorbed by the reference polymers PEUT and PIB. The unperturbed coating spectrum has been subtracted out in every case. Key spectral changes, marked by pointers, are discussed in the text. The asterisks mark negative peaks corresponding to Ni-Cam absorbances, indicating that sorption of DMMP diminishes the absorbance of NiPC at those frequencies.

Figure 12. IR reflectance spectra of: two different concentrations of pyridine (p/p_0 = 2.9 and 1.1%) interacting with Ni-Cam, labeled Ni-Cam 3 and Ni-Cam 1, as well as pyridine (p/p_0 = 2.9%) sorbed by the reference polymers PIB and PEUT. Key spectral changes, marked by pointers, are discussed in the text; note the appearance of a very intense band at 1527 cm^{-1}, attributable to changes in the β-

diketonate–Ni system as a consequence of coordination of the pyridine by the Ni.

Figure 13. IR reflectance spectra of pyrrole (p/p_0 = 5.3%) in the gas phase (using a gold blank; labeled "gas") and sorbed by Ni-Cam, as well as the reference polymer PIB (labeled Ni-Cam and PIB, respectively). Spectra are *p* polarized and the unperturbed coating spectrum has been subtracted out. No spectral changes are measurable—i.e., both spectra for sorbed pyrrole are identical to those for the free vapor—because pyrrole is a relatively weak Lewis base and so does not interact significantly with the Ni camphorate. Spectral lines resulting from contamination of the pyrrole source with water are indicated.

Figure 14. Normalized sensor responses upon exposure to a range of analytes of 97-MHz SAW devices incorporated in the reflectance IR substrate, coated with the selective, coordinatively unsaturated Ni camphorate complex depicted in Figure 2, as well as the conventional polymers PIB and PEUT.. Three responses per analyte were normalized to p/p_0, molecular weight, and the response to *n*-octane, then averaged, as detailed in the Figure 6 caption. Note the marked preference for the Lewis bases pyridine and *n*-butyl amine.

Table 1. TSMR partition coefficients, measured in the range p/p_0 = 0 – 0.2 %, along with saturation vapor pressures, of various analytes sorbed into PIB, PEUT, and the molecular recognition coating CD depicted in Figure 2. The "thermodynamically" normalized partition coefficients are calculated from the values in columns 3 - 5 by multiplication by the saturation vapor pressure in column 2 and division by the value of *n*-octane. These normalized values may be compared to the SAW data in Fig. 6.

Analyte	p_0 303 K [Pa]	Partition coefficient			Normalized Partition Coefficients		
		PIB	PEUT	CD	PIB	PEUT	CD
***n*-Octane**	*2430*	**1720** ± 30	**950** ± 30	**1780** ± 50	**1.0**	**1.0**	**1.0**
Toluene	*4820*	**1030** ± 20	**1750** ± 20	**2400** ± 80	**1.2**	**4.1**	**2.7**
Trichloromethane	*31900*	**200** ± 10	**850** ± 30	**1200** ± 50	**1.5**	**14**	**8.9**
Tetrachloroethene	*3160*	**2060** ± 30	**2050** ± 100	**2800** ± 150	**1.6**	**3.2**	**2.1**
Propan-1-ol	*3780*	**90** ± 5	**1380** ± 20	**1650** ± 50	**0.1**	**2.2**	**1.5**
Methyl 2-R-chloropropionate	*< 500*	**860** ± 10	**3300** ± 50	**38000** ± 1300	**0.1**	**0.9**	**4.4**
Methyl 2-S-chloropropionate	*< 500*	**860** ± 10	**3300** ± 50	**141000** ± 3500	**0.1**	**0.9**	**16.4**
R-Methyl lactate	*830*	**570** ± 20	**5400** ± 200	**83600** ± 2000	**0.1**	**2.7**	**16.1**
S-Methyl lactate	*830*	**570** ± 20	**5400** ± 200	**59000** ± 1500	**0.1**	**2.7**	**11.4**
Water (50% RH)	*4180*	--	**330** ± 5	**410** ± 20	--	**0.6**	**0.4**

Table 2. TSMR partition coefficients, measured in the range p/p_0 = 0 – 0.2 %, along with saturation vapor pressures, of various analytes sorbed into PIB, PEUT and the molecular recognition coating NiPC depicted in Figure 2. The "thermodynamically" normalized partition coefficients are calculated from the values in columns 3 - 5 by multiplication by the saturation vapor pressure in column 2 and division by the value of *n*-octane. These normalized values may be compared to the SAW data in Fig. 9.

Analyte	p_0 303 K [Pa]	Partition coefficient			Normalized Partition Coefficients		
		PIB	PEUT	NiPC	PIB	PEUT	NiPC
***n*-Octane**	*2430*	1720 ± 30	950 ± 30	720 ± 20	1.0	1.0	1.0
Trichloromethane	*31900*	200 ± 10	850 ± 30	290 ± 10	1.5	14	5.4
Tetrachloroethene	*3160*	2060 ± 30	2050 ± 100	2100 ± 50	1.6	3.2	3.9
Propan-1-ol	*3780*	90 ± 5	1380 ± 20	950 ± 30	0.1	2.2	2.1
Benzene	*15700*	360 ± 10	710 ± 20	3500 ± 100	1.4	5.4	32
Toluene	*4820*	1030 ± 20	1750 ± 20	11000 ± 500	1.2	4.1	31
***m*-Xylene**	*1460*	3400 ± 50	5200 ± 200	17500 ± 1000	1.2	3.5	15
Pyridine	*3570*	480 ± 20	3600 ± 200	10200 ± 200	0.4	5.8	21
Tetrahydrofuran	*29000*	220 ± 5	420 ± 20	190 ± 10	1.5	5.5	3.2

Table 3. TSMR partition coefficients, measured in the range p/p_0 = 0 – 0.2 %, along with saturation vapor pressures, of various analytes sorbed into PIB, PEUT and the molecular recognition coating Ni-Cam depicted in Figure 2. The "thermodynamically" normalized partition coefficients are calculated from the values in columns 3 - 5 by multiplication by the saturation vapor pressure in column 2 and division by the value of *n*-octane. These normalized values may be compared to the SAW data in Fig. 14.

Analyte	p_0 303 K [Pa]	Partition coefficient			Normalized Partition Coefficients		
		PIB	PEUT	Ni-CAM	PIB	PEUT	Ni-CAM
***n*-Octane**	*2430*	**1720** ± 30	**950** ± 30	**250** ± 10	**1.0**	**1.0**	**1.0**
Toluene	*4820*	**1030** ± 20	**1750** ± 20	**650** ± 20	**1.2**	**4.1**	**5.2**
Tetrachloroethene	*3160*	**2060** ± 30	**2050** ± 100	**810** ± 20	**1.5**	**14**	**4.3**
Propan-1-ol	*3780*	**90** ± 5	**1380** ± 20	**1600** ± 30	**0.1**	**2.2**	**10**
Tetrahydrofuran	*29000*	**220** ± 5	**420** ± 20	**800** ± 30	**1.6**	**3.2**	**38**
Pyridine	*3570*	**480** ± 20	**3600** ± 200	**37000** ± 1000	**0.4**	**5.8**	**220**
n-Butylamine	*15300*	**220** ± 10	**750** ± 20	**73000** ± 2000	**0.8**	**5.2**	**1800**
Pyrrole	*1480*	**810** ± 20	**11500** ± 500	**3100** ± 100	**0.3**	**7.7**	**7.6**
Water (50% RH)	*4180*	--	**330** ± 5	**860** ± 20	--	**0.6**	**5.9**

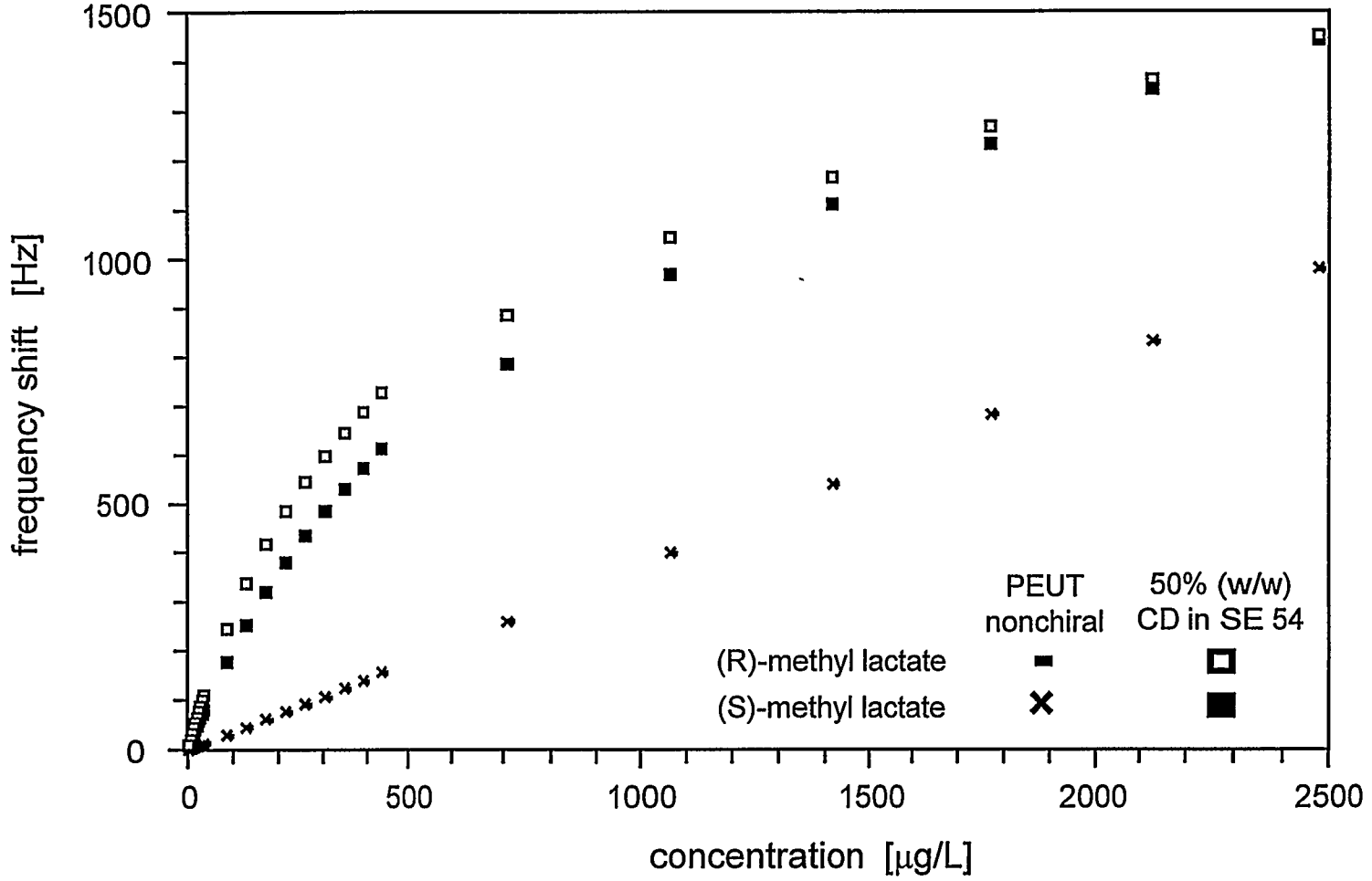

Hierlemann et al. Fig. 1

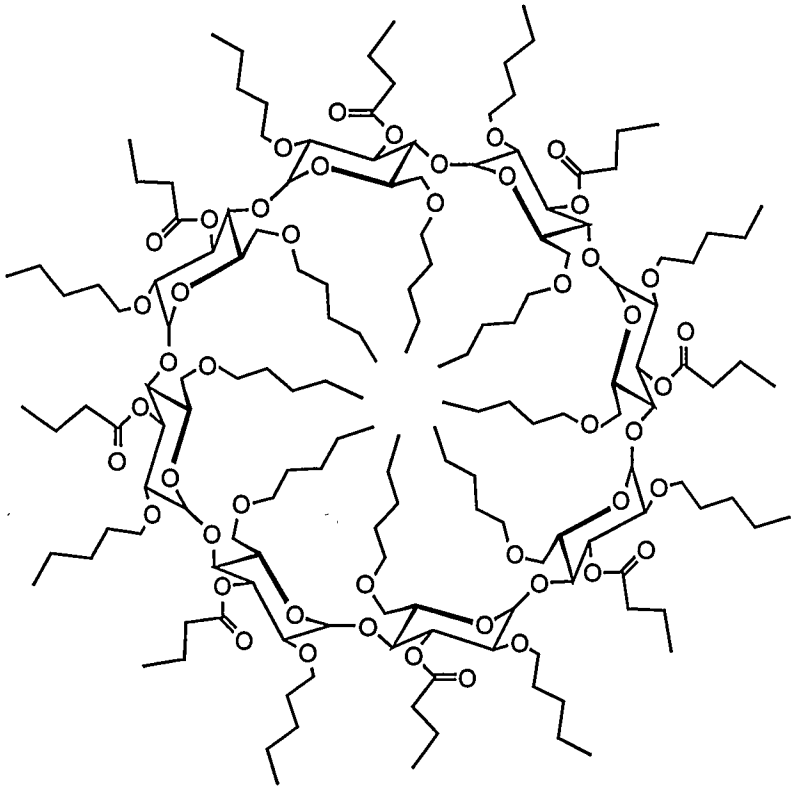

modified cyclodextrin

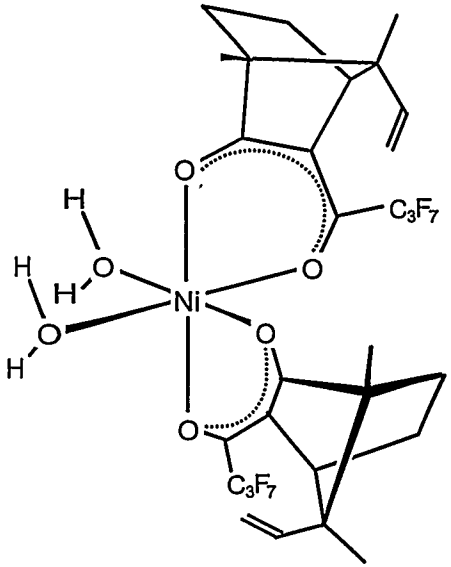

nickel camphorate

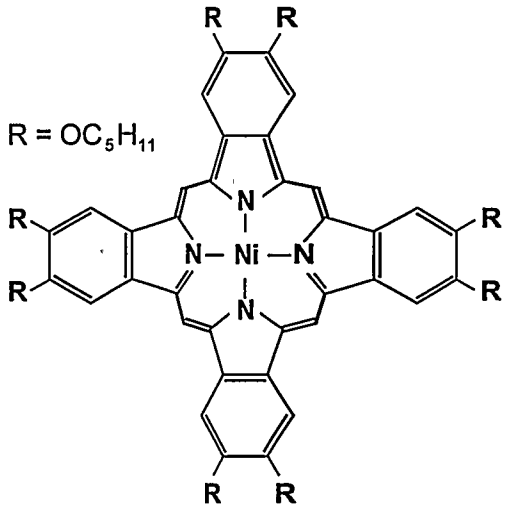

nickel phthalocyanine

Hierlemann et al. Fig. 2

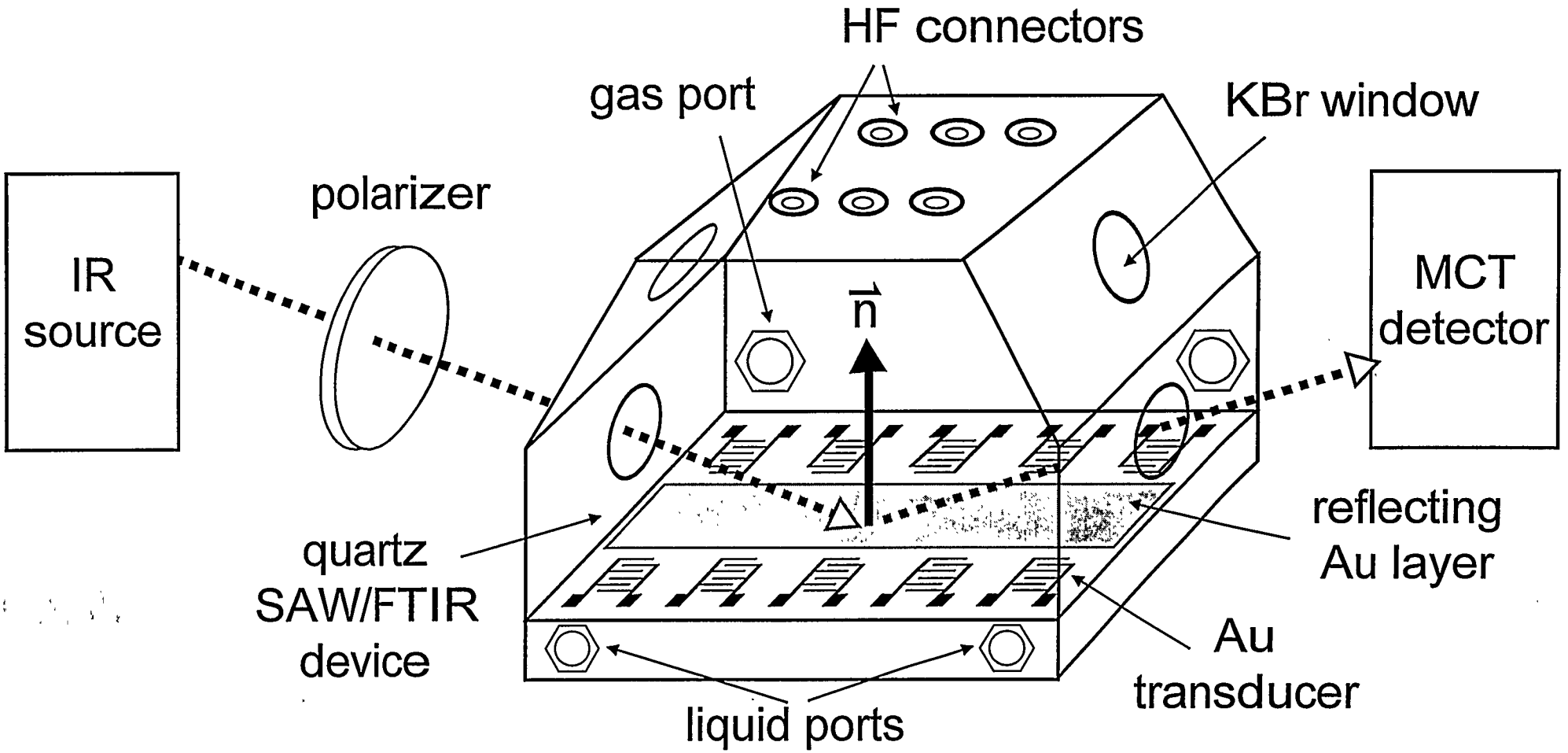

Hierlemann et al. Fig. 3

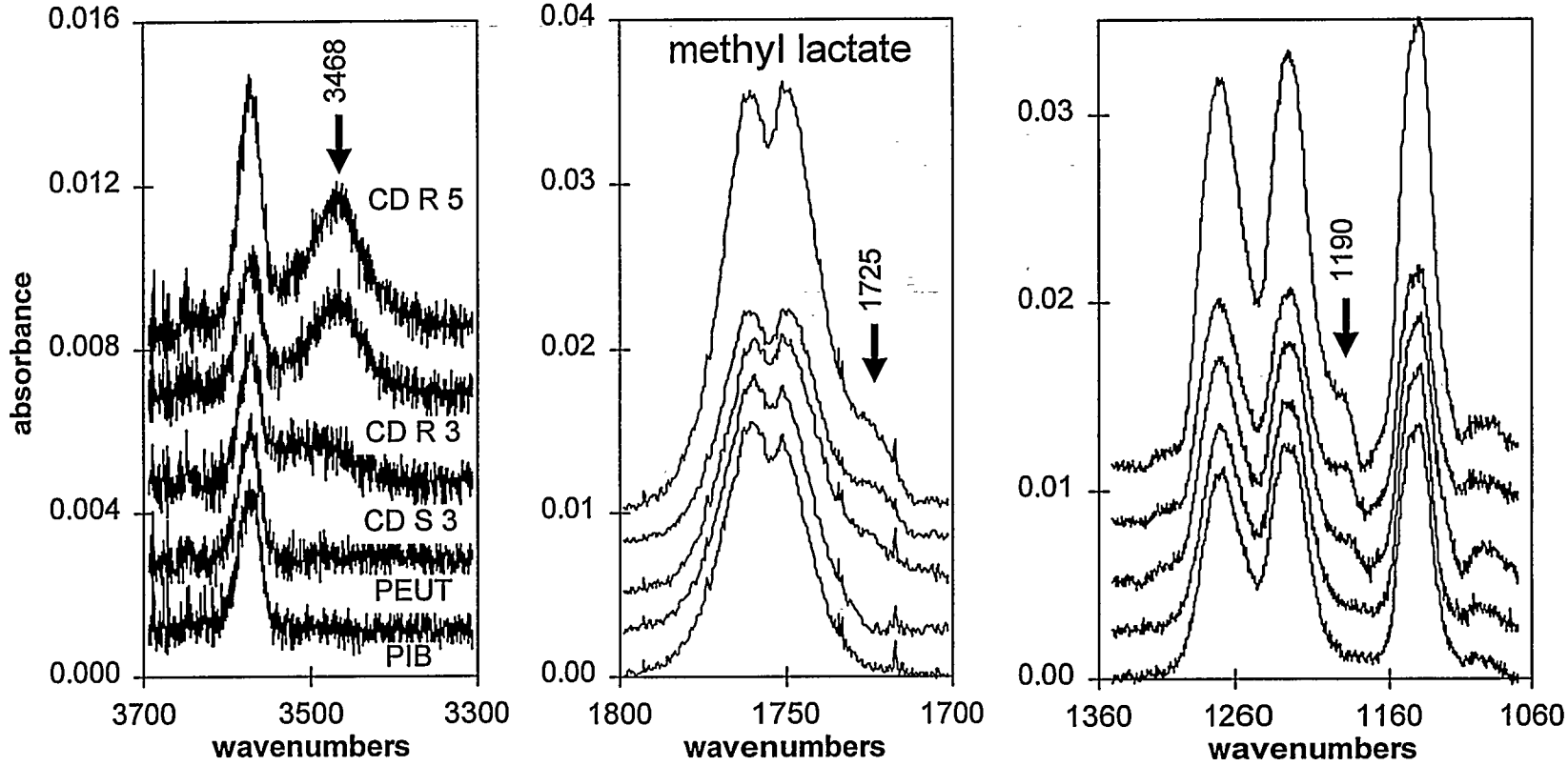

Hierlemann et al. Fig. 4

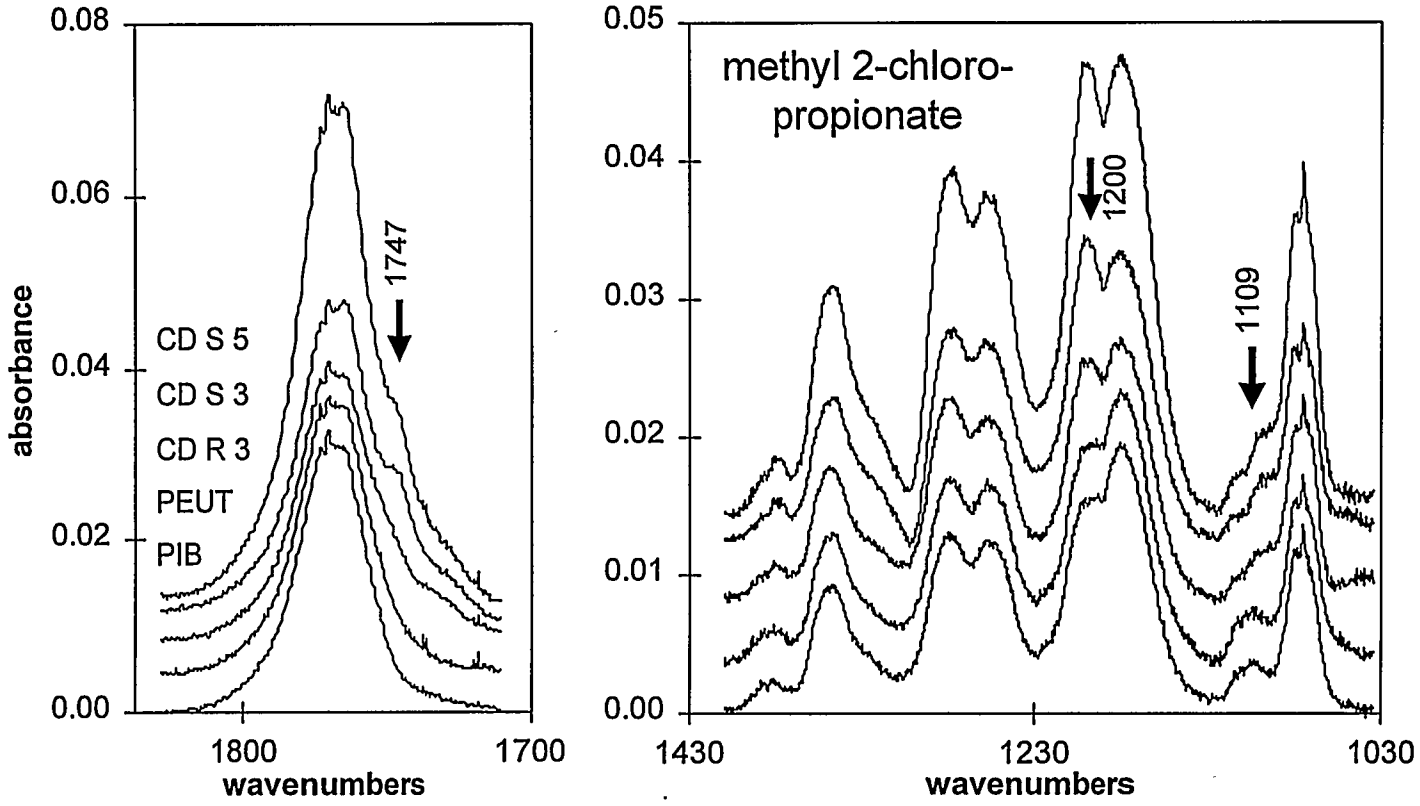

Hierlemann et al. Fig. 5

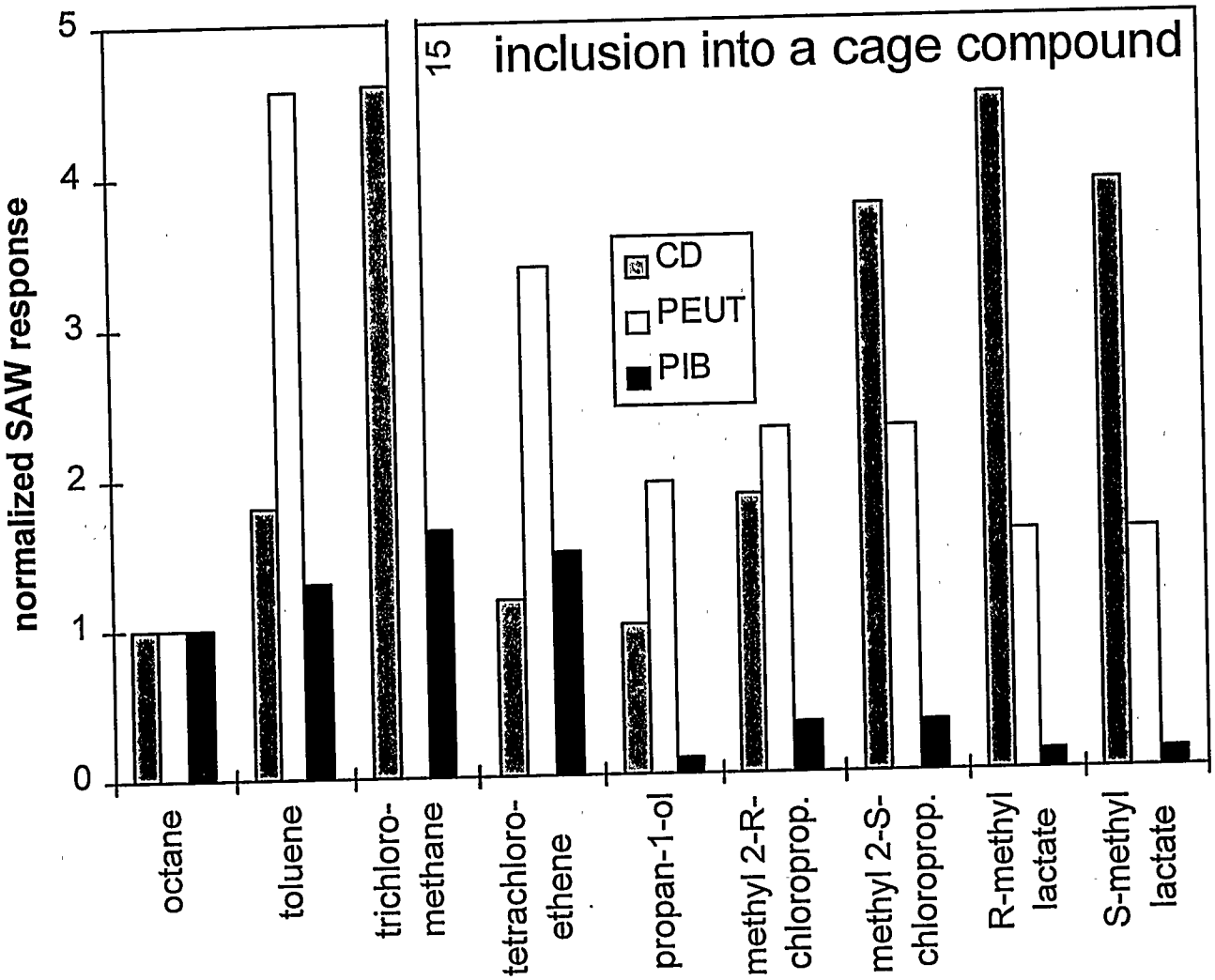

Hierlemann et al. Fig. 6

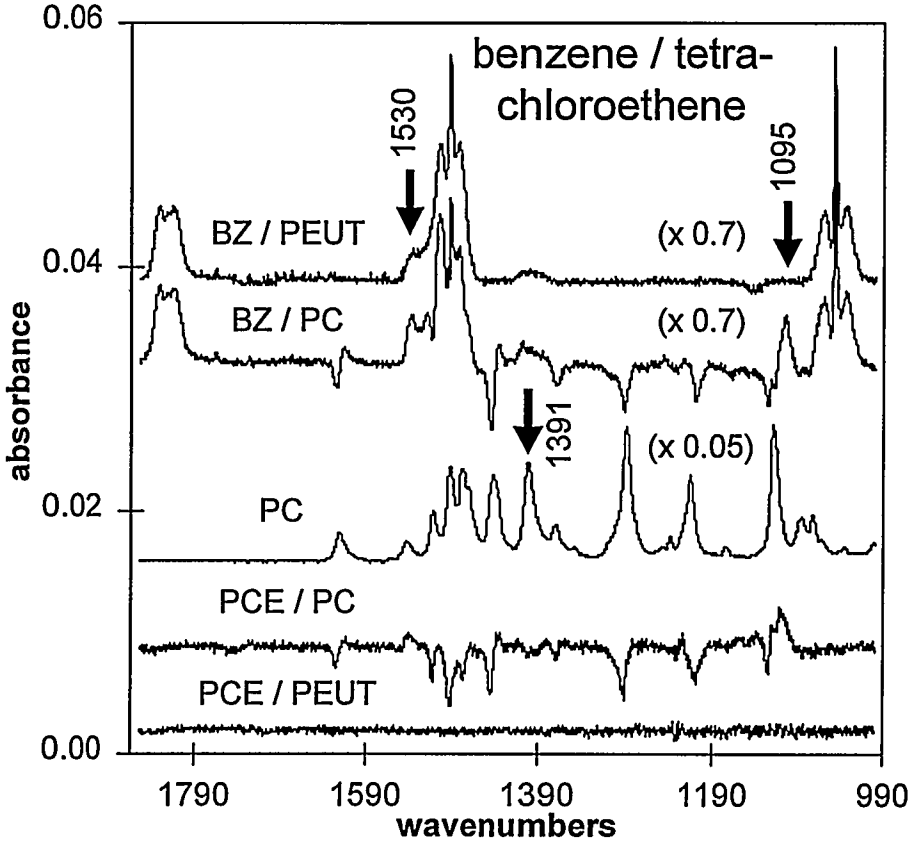

Hierlemann et al. Fig. 7

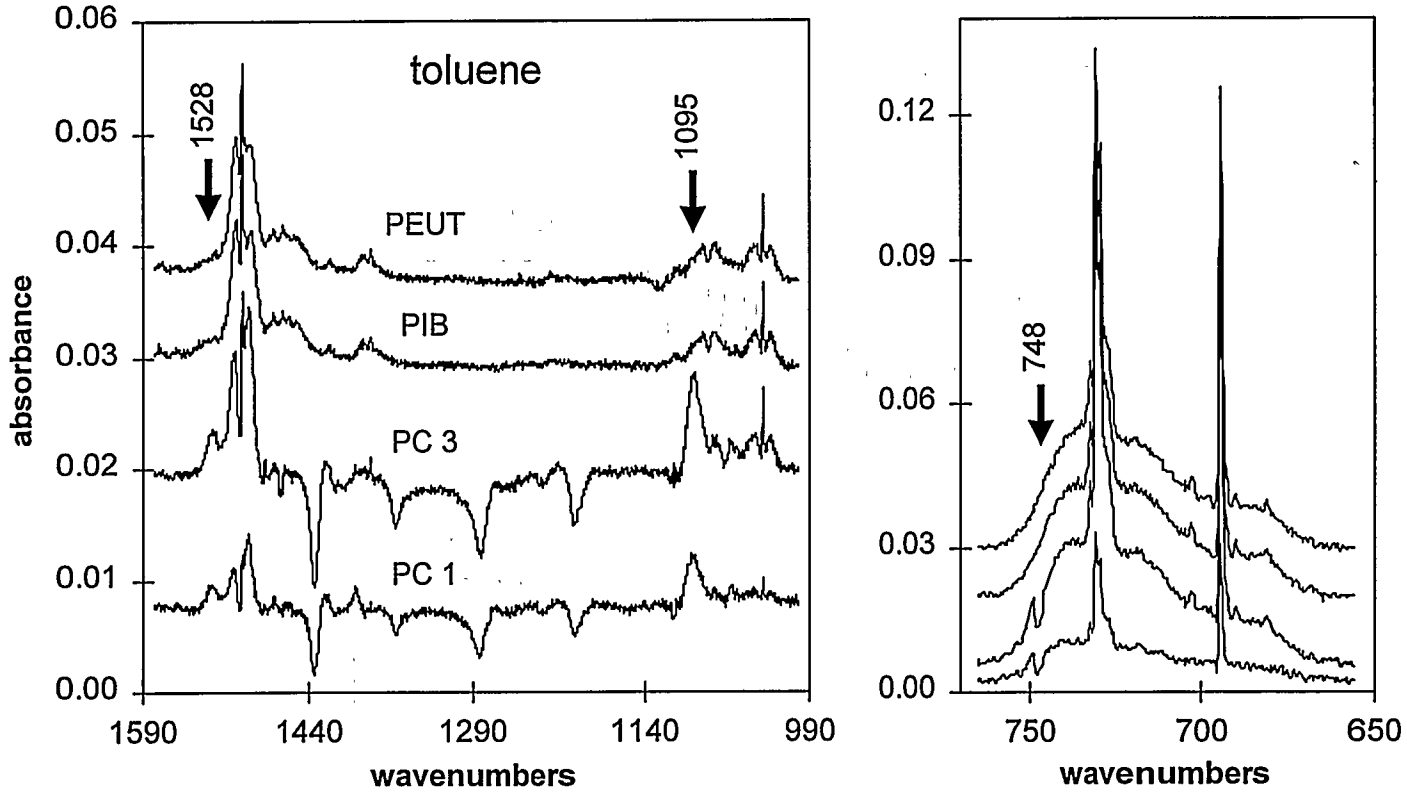

Hierlemann et al. Fig. 8

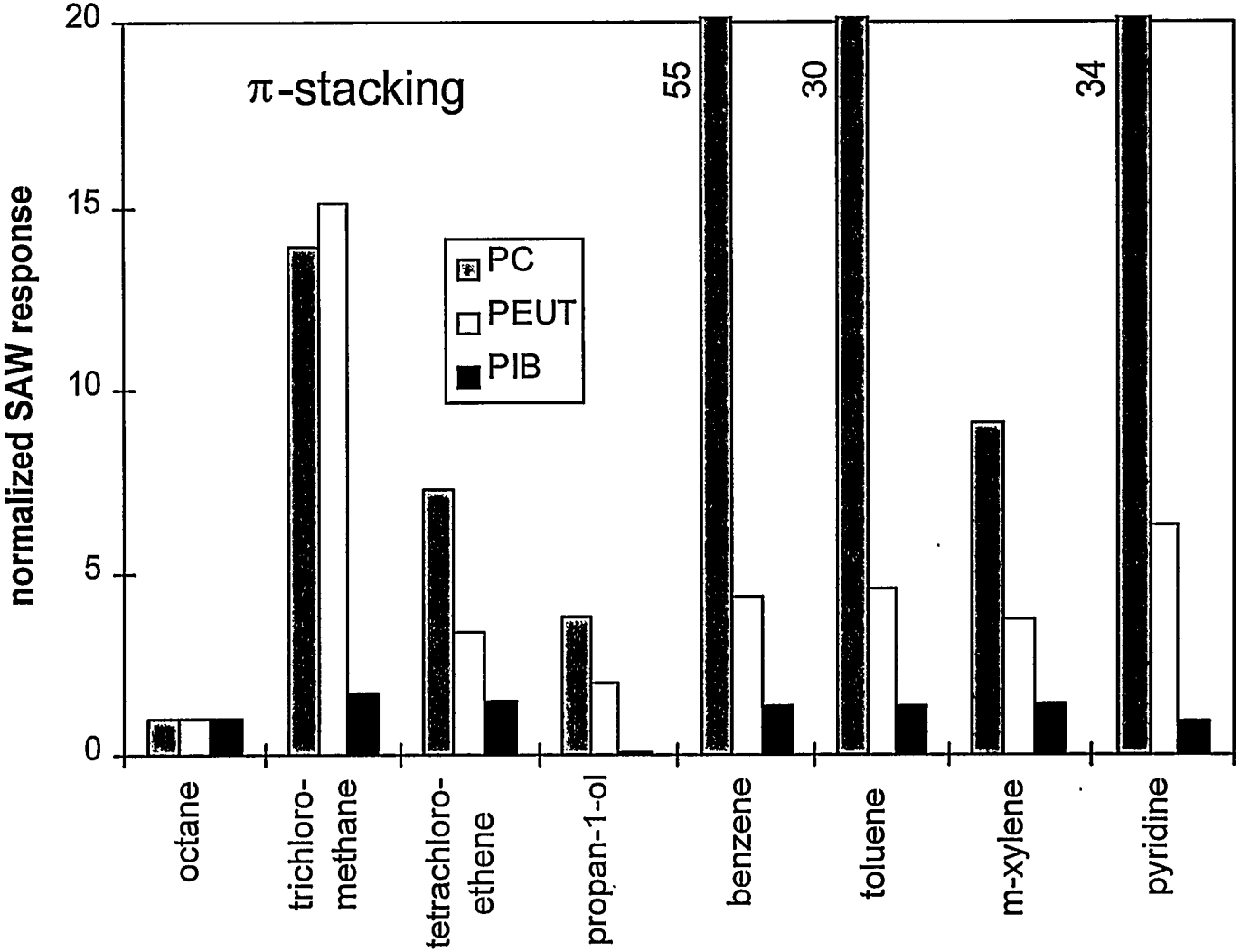

Hierlemann et al. Fig. 9

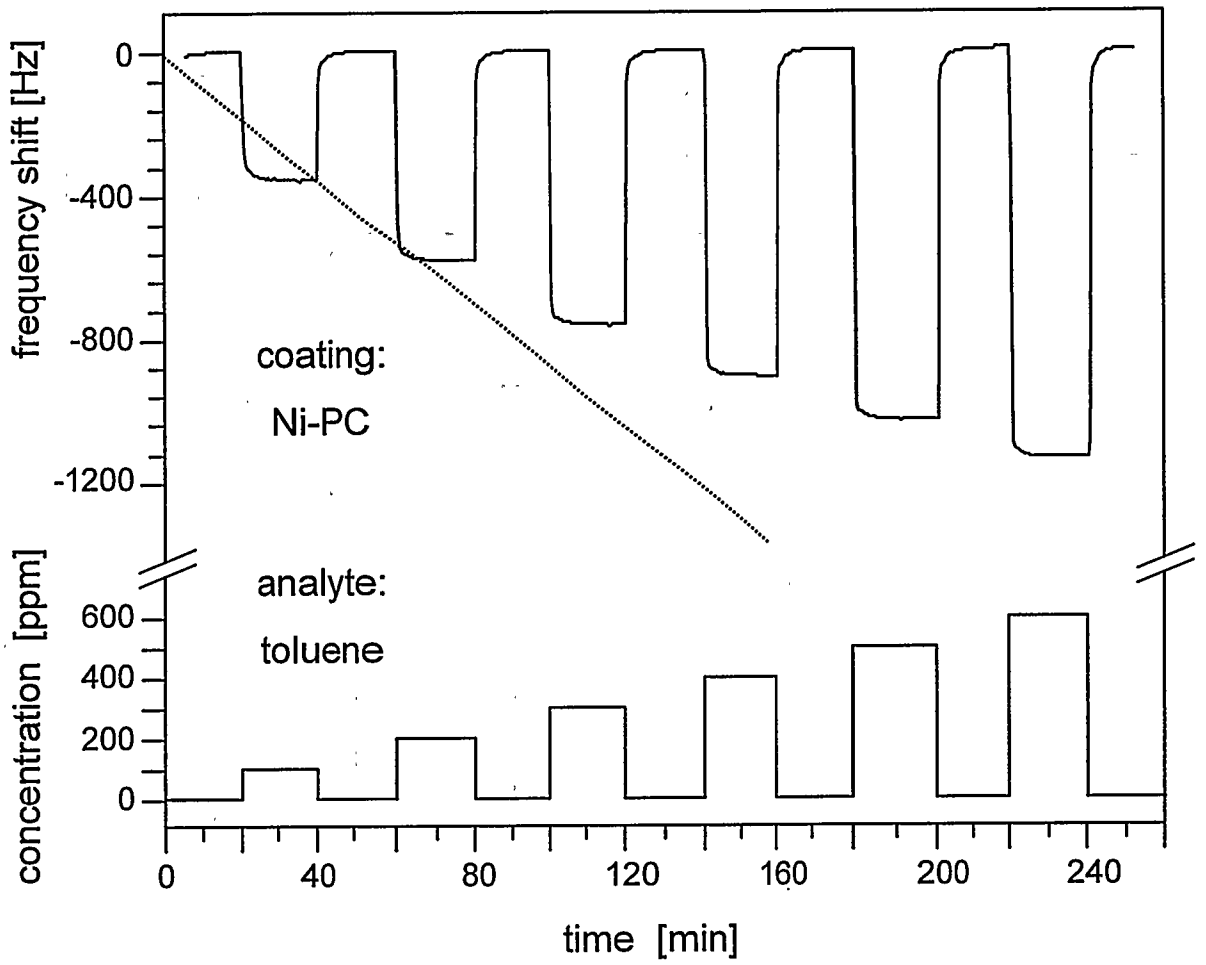

Hierlemann et al. Fig. 10

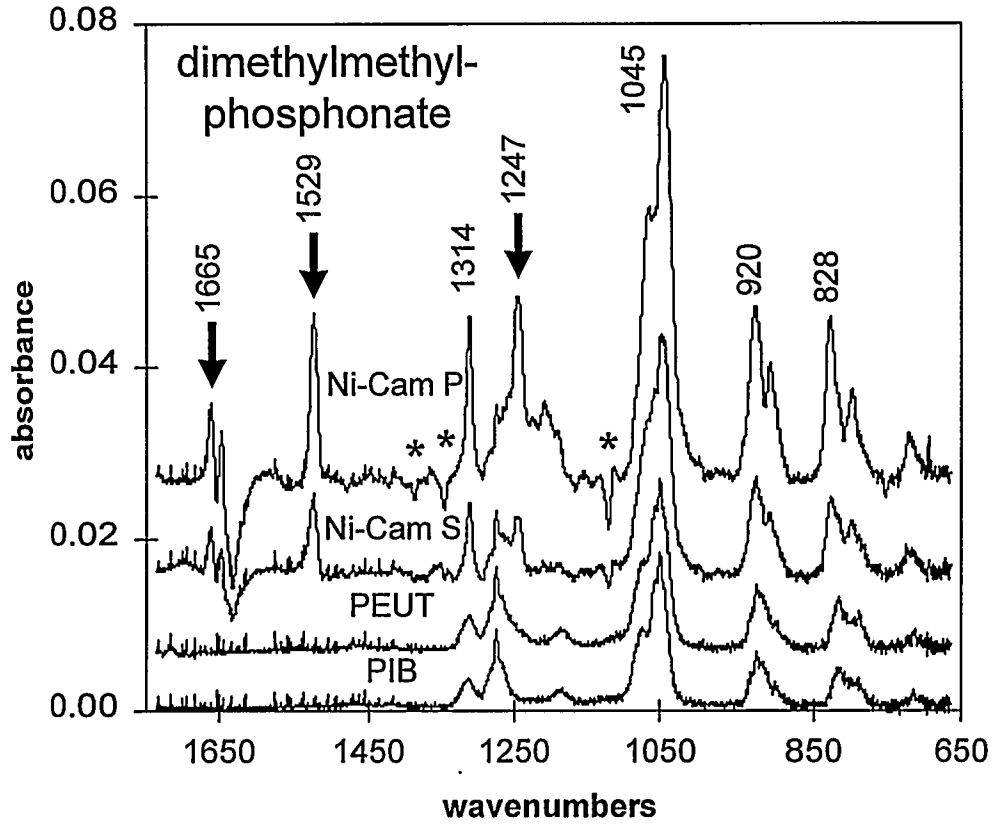

Hierlemann et al. Fig. 11

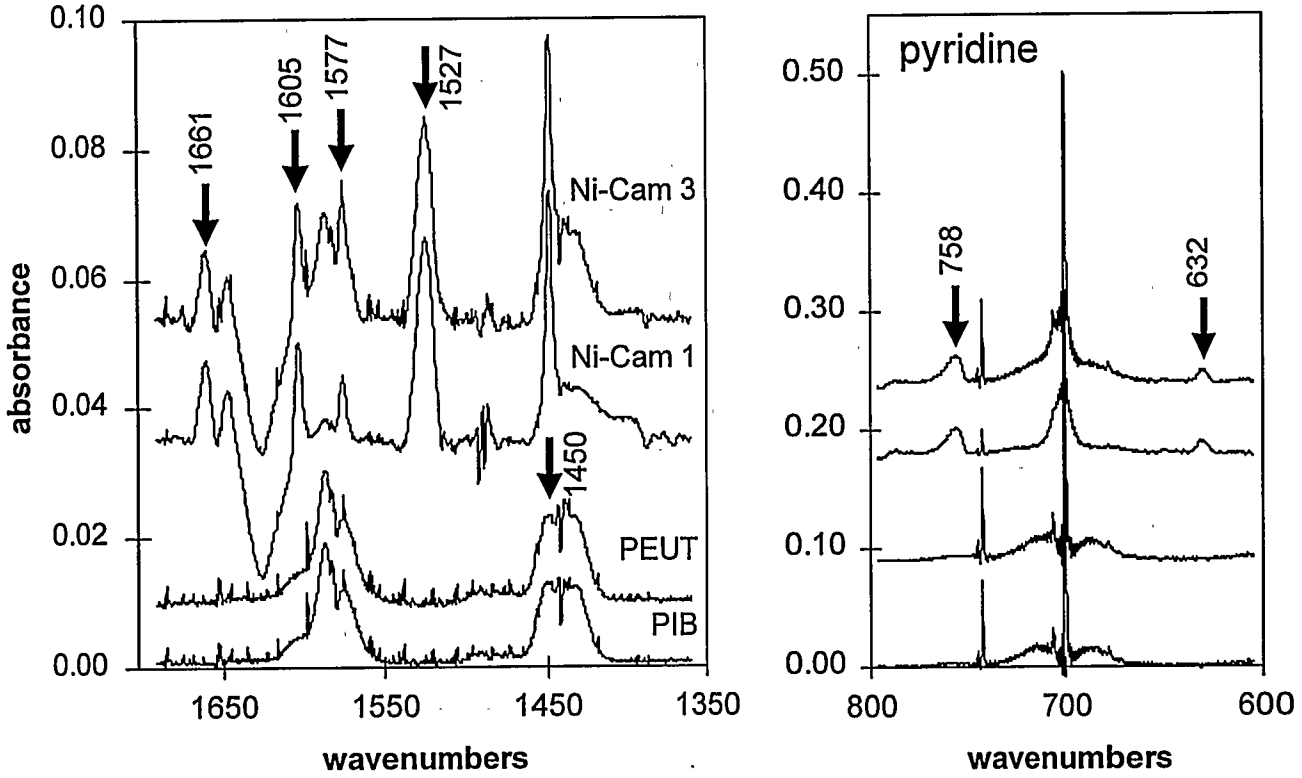

Hierlemann et al. Fig. 12

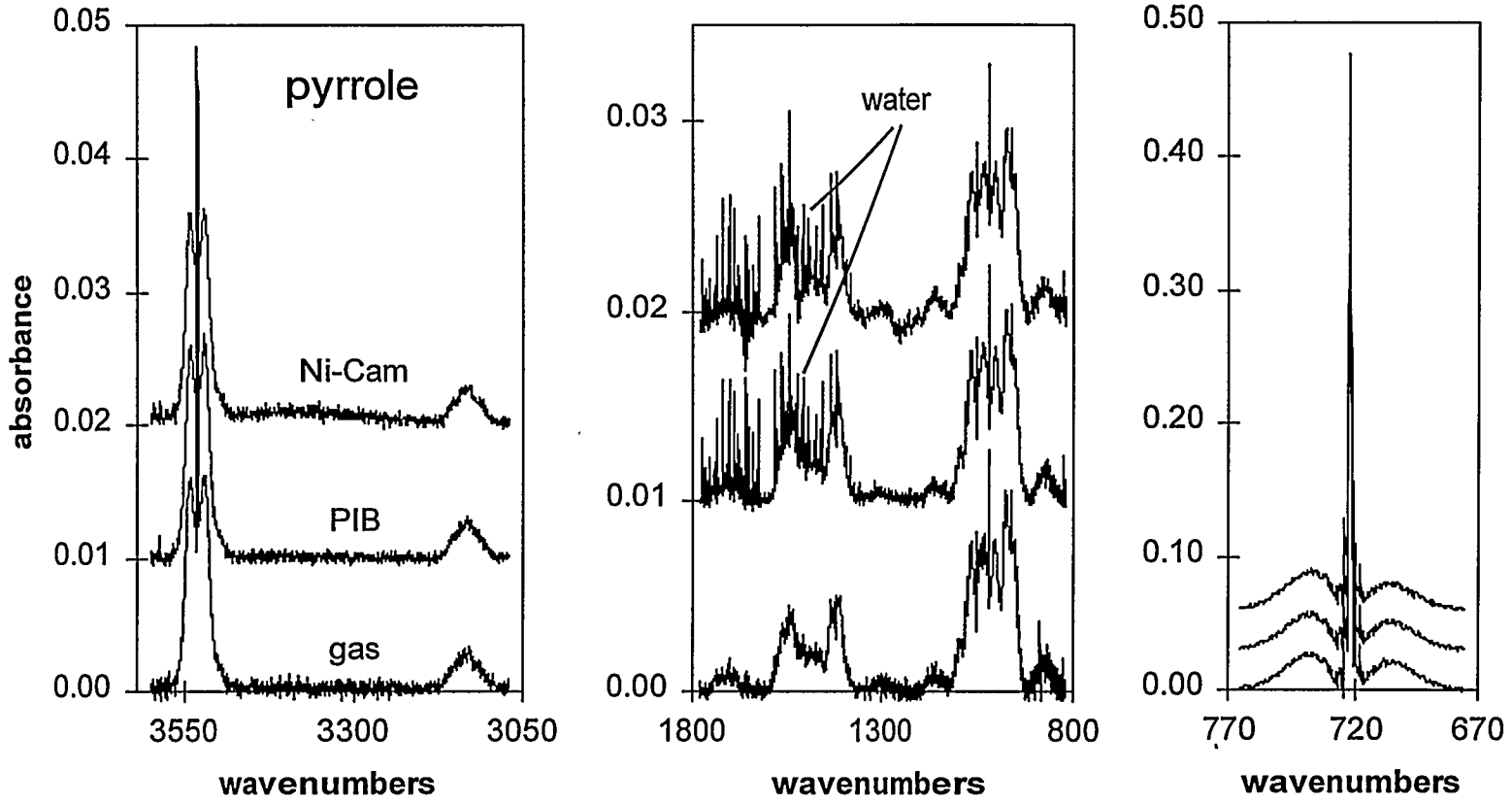

Hierlemann et al. Fig. 13

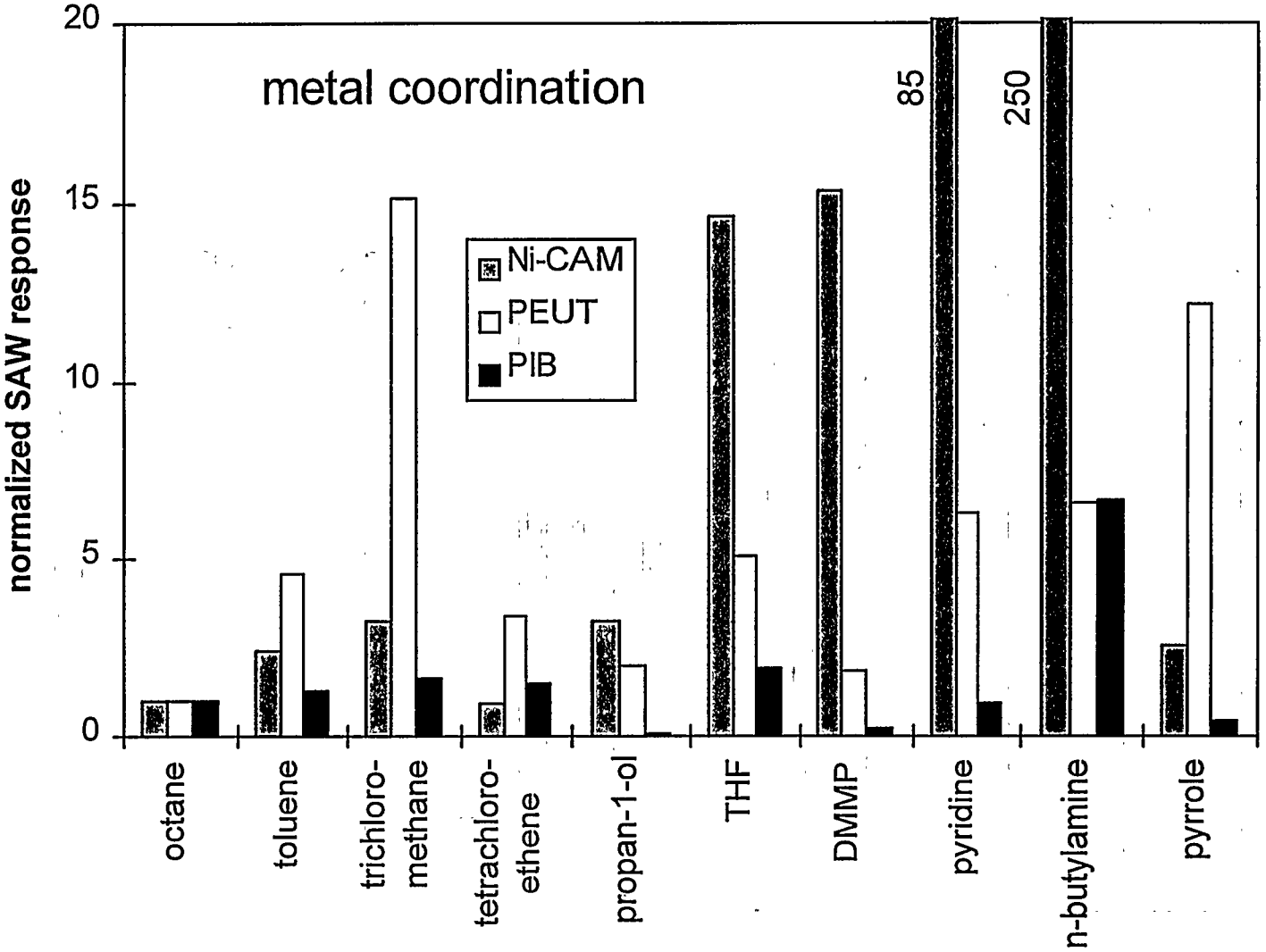

Hierlemann et al. Fig. 14